May 2023

Organic Fouling Behavior and Mechanisms in Nanofiltration Membranes for Water Treatment Processing

Sydney Rose Morgan
University of Wisconsin-Milwaukee

ORGANIC FOULING BEHAVIOR AND MECHANISMS IN NANOFILTRATION MEMBRANES FOR WATER TREATMENT PROCESSING

by

Sydney Morgan

A Thesis Submitted in

Partial Fulfillment of the

Requirements for the Degree of

Master of Science

in Engineering

at

The University of Wisconsin-Milwaukee

May 2023

ABSTRACT

ORGANIC FOULING BEHAVIOR AND MECHANISMS IN NANOFILTRATION MEMBRANES FOR WATER TREATMENT PROCESSING

by

Sydney Morgan

The University of Wisconsin-Milwaukee, 2023
Under the Supervision of Professor Yin Wang

Nanofiltration membrane technology is an expanding topic of interest for use in water treatment processes, particularly in the elusive field of desalination. Desalination is becoming more and more necessary as climate-change related weather events like droughts, and populations in water scare areas both increase. Reverse osmosis membrane systems are a reliable, but costly method for removing salts from otherwise unusable saline water sources. One way to decrease the cost of these systems is by utilizing porous membranes, like ultrafiltration or nanofiltration membranes, for pretreatment. Additionally, nanofiltration has recently shown promise as an effective alternative to reverse osmosis in desalination systems.

The main cause of concern in membrane systems is fouling, which has many different causes and manifestations in real-world scenarios. Fouling causes a decline in the membrane's flux over time and lowers the membrane's lifespan. A more robust understanding of the many complexities of membrane fouling can help to better prevent and treat fouling in a system. This can reduce the overall system costs by reducing cleaning time, increasing membrane lifespans, and decreasing energy requirements. This study compared two nanofiltration membranes – commercially manufactured NF270 membranes, and lab-synthesized Covalent Organic Framework (COF) membranes – analyzing their fouling behaviors and mechanisms, during high-

concentration organic fouling. Fouling rate, fouling mechanisms and models, and limiting flux were explored.

To
my fiancé, Michael

TABLE OF CONTENTS

LIST OF FIGURES

LIST OF TABLES

LIST OF ABBREVIATIONS

BSA	Bovine serum albumin
COF	Covalent Organic Framework
DI	Deionized
DOI	Department of Interior
DWPR	DOI Desalination and Water Purification Research Program
LMH	Liters per square meter hour
MPa	Mega pascal
PAHA	Pre-treated Aldrich humic acid
Psi	Pounds per square inch
SRHA	Suwanee River Humic Acid

ACKNOWLEDGEMENTS

First and foremost, I would like to thank my advisor, Dr. Yin Wang for his help and encouragement through my master's studies and research over the past two years. I would also like to thank my committee member Dr. Xiaoli Ma for his expertise and advice throughout this project. I would particularly like to thank Rahul Khandge and Dr. Thanh Nguyen for their help in aiding in my experimental setup as well as for synthesizing the membranes used in this study. Dr. Nguyen was an exceptionally useful resource with his extensive experience and knowledge in the field. And to Rahul, I send my gratitude and regards as he continues this project along the journey toward his doctorate. Finally, I would like to thank the Department of Interior Desalination and Water Purification Research Program (DWPR) for graciously funding this research in order to further desalination research and advancements.

Chapter 1: Introduction

Climate change, increased drought events and drought severity, and population increases will bring about a continued decline in water availability across the world. Much of the United States is already experiencing water scarcity [1, 2, 3]. Novel methods of potable water production and water reclamation are critical to serve current and future populations. Desalination, the removal of salts from seawater or brackish groundwater, has been identified as having the potential to be a key player in future potable water production, particularly in areas of the United States already low on water supplies [1, 3]. Luckily, many areas of the United States that experience scarcity of traditional water sources tend to be abundant in saline water sources (i.e., California, Texas, Florida, etc.) [4].

1.1 Desalination: History and Policy

Desalination is the removal of salt from saline or biologically impaired waters in order to modify the water for a beneficial use. In many areas in the United States and around the world, freshwater is scarce. Desalination allows for the use of abundant seawater and brackish groundwater as potable water. The first municipal desalination plant for the production of potable water was built in 1954. This plant used a desalination process known as electrodialysis, but did not gain popularity due to its inability to reduce dissolved solids to a reasonable degree. Reverse osmosis membrane filtration is presently the most popular desalination method, but other methods – like nanofiltration – are being researched and produced in the hopes of lowering the energy requirements of large-scale desalination associated with reverse osmosis [1].

The Water Desalination Act of 1996 is the primary focal point of desalination policy across the United States. The law enacts that the Secretary of Interior can provide grants and contracts for the research and study of various topics in desalination [5]:

i. "Investigating desalination processes;
ii. Ascertaining the optimum mix of investment and operating costs;
iii. Ascertaining the optimum mix of investment and operating costs;
iv. Determining the best designs for different conditions of operation;
v. Investigating methods of increasing the economic efficiency of desalination processes through dual-purpose co-facilities with other processes involving the use of water;
vi. Conducting or contracting for technical work …;
vii. Studying methods for the recovery of byproducts resulting from desalination to offset the costs of treatment and to reduce environmental impacts from those byproducts; and
viii. Salinity modeling and toxicity analysis of brine discharges, cost reduction strategies for constructing and operating desalination facilities, and the horticultural effects of desalinated water used for irrigation."

Through funding from the Infrastructure Investment and Jobs Act of 2021 (commonly referred to as the Bipartisan Infrastructure Law) grants and loans can be distributed for a variety of drinking water, stormwater, and water reclamation related studies and projects. The law provides $1 billion federally over five years for water reclamation and reuse projects, including $250 million specifically for water desalination projects and studies in accordance with the Water Reclamation Act of 1996 [6].

Additionally, the Department of Interior (DOI) provides research grants for desalination projects through the Desalination and Water Purification Research Program (DWPR). The DWPR

funds reclamation research with the aims to "develop more innovative, cost effective, and technologically efficient ways to desalinate water." The overall goal of this program is to reduce the economic and environmental impacts of treating impaired waters [7].

California, Florida, and Texas are leading states in the desalination sector. All three states have suffered from exceptional droughts to varying extents since the early 2010s. Additionally, Florida and California are among the largest agricultural producers in the United States, making water availability for that purpose crucial. All three states experience low, and continuously declining, availability of traditional water sources (particularly fresh surface water) compared to their respective populations [4, 8, 9, 10].

Desalination has been used in all three states as a way to combat water scarcity, depleting surface and groundwater sources, and drought. Even with all three states' proximity to seawater, the vast majority of desalination across the board has been with brackish groundwater and saline river water. Desalination of seawater is muchmore expensive in terms of cost and energy expenditure because it has a much higher concentration of salts than brackish water. With further technological advances, seawater desalination can become more viable across the states, particularly in water-scarce areas [4].

J.R. Ziolkowska and R. Reyes performed a SWOT (Strengths, Weaknesses, Opportunities, and Threats or Challenges) analysis of the prospects of the desalination sector in the United States. The key strength associated with the desalination sector is the ability to utilize additional abundant sources of water with the removal of salt from brackish water and seawater. On the other hand, the main weakness regarding desalination is the relatively high cost compared to other water sources due to high energy requirements. Much of the current research and innovations in desalination is in the hopes of lowering the costs associated with treatment. Some opportunities for the sector are

the abundance of saline waters and the large quantity of federal and state grants and loans for research and development. Finally, threats to or challenges faced by the desalination sector include the volatility of energy prices (hopefully the increased use of renewable energies could remedy this) and a low social awareness about the need for additional water sources due to the paradoxically low price of water compared to the high cost of water production and treatment [4].

Innovations in membrane filtration technologies have the potential to lower energy requirements associated with conventional reverse osmosis desalination. For example, novel nanofiltration and ultrafiltration membranes have the potential to replace costly reverse osmosis processes, or act as a pretreatment with the goal of reducing the overall process costs [1].

1.2 Pressure-Driven Membrane Technologies

A membrane is defined as a barrier which separates two phases and restricts the transport of components in a selective manner. Conventional filters meet this simple definition, but the term filter is generally reserved for structures that separate particles one to ten microns or larger. Membranes technologies typically select for much smaller particles. The main benefit of using membrane systems for water treatments, particularly desalination, is that membranes can employ highly selective separation. The size of particles the membrane restricts is dependent on the type of membrane (Figure 1). There are four main types of synthetic pressure-driven membrane technologies: reverse osmosis, nanofiltration, ultrafiltration, and microfiltration [1, 11].

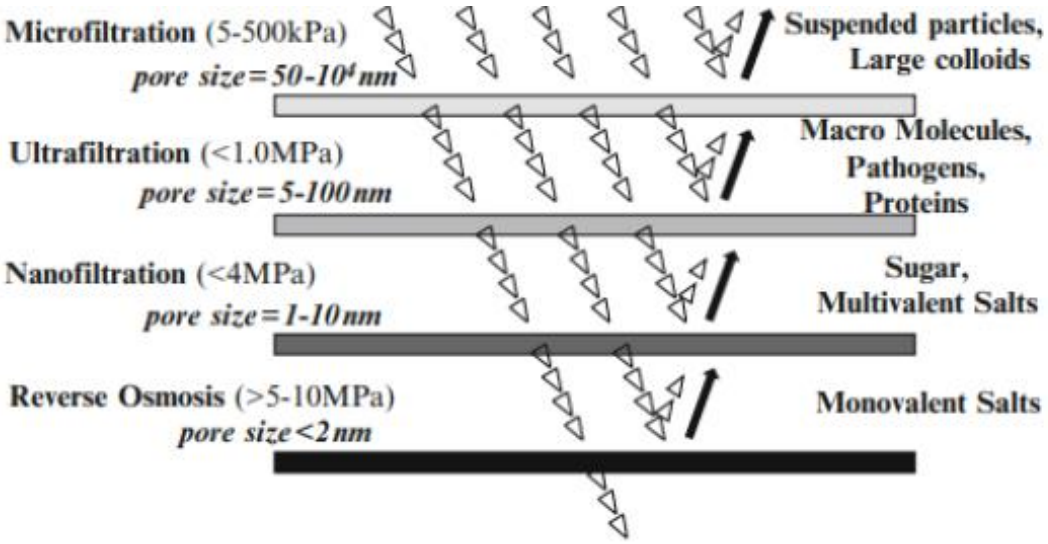

Figure 1 Pressure-driven membranes for water and wastewater treatments [1].

A synthetic membrane can fall into several classifications which describe its driving force, configuration, and structure. A membrane can be organic (polymeric) or inorganic (ceramic or metal), solid or liquid, electrically charged or neutral, homogeneous or heterogeneous, and symmetrical or asymmetrical (Figure 2) [1].

Pressure is the driving force of modern membrane desalination systems. Broadly, pressure-driven membranes can be categorized as low-pressure membranes (microfiltration and loose ultrafiltration) or high-pressure membranes (tight ultrafiltration, nanofiltration, and reverse osmosis) [11].

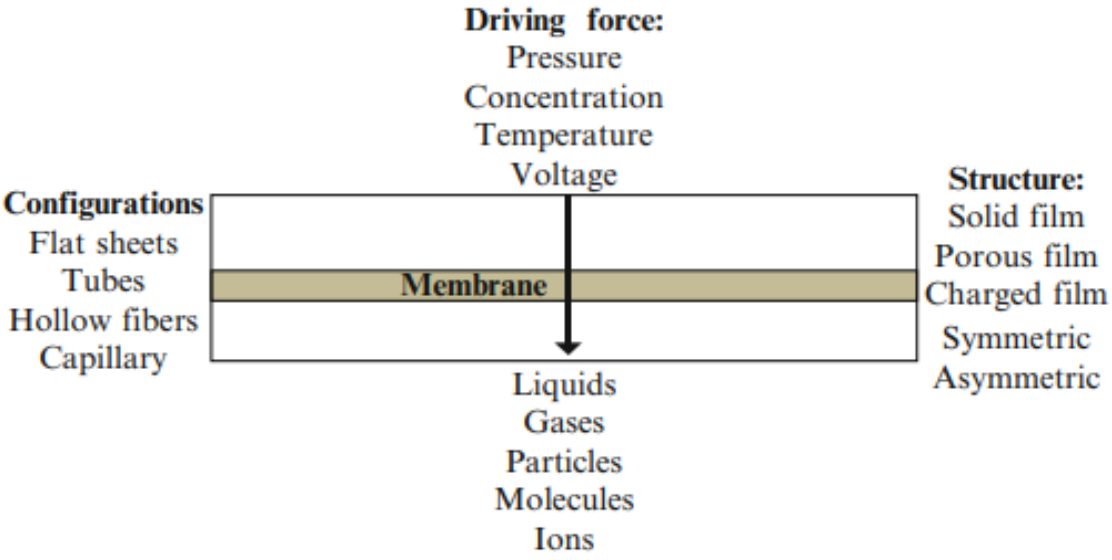

Figure 2 Fundamentals of membrane and membrane processes [1].

Cost is an important factor to consider when designing a desalination system and is often a limiting factor for municipalities. Desalination systems are often rejected by municipalities, even when traditional water sources are scarce, in favor of shipping in water from great distances due to the energy requirements and high costs associated with desalination, and the relatively low cost of water shipment [12]. The factors that govern operating costs of a membrane system include power requirements, labor, materials, membrane cleaning, scale inhibition (reduction in crystal formation), and membrane replacement. Additionally, a major obstacle for membrane systems is the potential for rapid decline of the permeate flux due to membrane fouling [11, 13, 14]. All of these factors must be considered when designing a lasting and sustainable membrane system.

1.2.1 Reverse Osmosis

Osmosis is a natural phenomenon that has been studied since the 18th century. In 1748, the permeation of water through a pig's bladder covering a jar of wine was discovered accidentally by Abbé Nollet. Osmosis is the diffusion of a fluid (typically water) through a semipermeable membrane from a low solute concentration solution on one side of the membrane, to a high solute

concentration solution on the other side until an equilibrium of solute concentration is reached on both sides. The pressure difference between the two sides of the membrane is known as osmotic pressure. During osmosis, this pressure gradient acts as the driving force for the fluid transfer [1].

If an external pressure higher than the osmotic pressure is applied, the fluid can flow from the high solute concentration side of the membrane to the low solute concentration side. This can fully separate the fluid from the solute. This process is known as reverse osmosis (also referred to as "hyperfiltration"). The first reverse osmosis membrane prototypes were developed in the 1920s by L. Michaelis and E. Manegod. Reverse osmosis membranes are typically considered nonporous, with pores less than two nanometers in size and operate at high working pressures of five to ten MPa (Figure 1). Reverse osmosis applications in the desalination industry include potable water production, seawater purification, brackish water purification, and municipal wastewater reclamation [1].

1.2.2 Nanofiltration

Nanofiltration technology started laboratory development in the 1980s. Nanofiltration membranes were originally described as a subset of reverse osmosis processes that selectively and purposefully allows for the permeation of some ionic solutes. However, according to Wang, et al. [1], "…different from [reverse osmosis] membranes which [have a] nonporous structure and a transport mechanism of solution-diffusion, [nanofiltration] membranes operate at the interface of porous and nonporous membranes with both sieving and diffusion transport mechanisms." Thus, nanofiltration membranes share qualities with both the nonporous diffusion seen with reverse osmosis, and the porous filtration seen with ultrafiltration and microfiltration. Nanofiltration membrane pores range from one to ten nanometers in size and operate as a pressure less than four MPa (Figure 1) [1].

Nanofiltration membranes are often, but not always, characterized by a charged surface which allows electric interactions to add to the selective rejection behavior, high permeability of monovalent salts, the near-complete elimination of multivalent salts, the removal of small organic compounds, and the liability to fouling [1]. Membrane fouling is a key issue that is central to much of modern membrane research from the past two decades.

Nanofiltration membranes are gaining popularity in desalination treatment processes and are particularly popular as a pretreatment to reverse osmosis desalination treatment, especially as a seawater softening treatment [1]. Nanofiltration membranes can remove turbidity, nitrates, hardness, and dissolved salts. When used as pretreatment, the feed water can be purified to a quality more acceptable to the reverse osmosis membranes. This pretreatment can help to reduce the system's overall energy consumption, making the system ultimately more environmentally friendly, sustainable, and cost effective. Additionally, with the addition of nanofiltration purification, fouling potential can be reduced in the system, leading to increased membrane lifespans and the reduction in system downtime for necessary membrane cleaning. The conventional pretreatment used prior reverse osmosis is typically media filtration, but this method can be lacking due to inconsistent performance and lower selectivity. New treatment and pretreatment methods using nanofiltration are considered a breakthrough in modern desalination processes [15, 16].

More recently, nanofiltration technology has been shown to be as effective as a primary desalination treatment as reverse osmosis, and at times even more efficient. Wafi, et al. found that when used for desalination, nanofiltration membranes produced comparable quality water with 29% lower energy consumption [16].

1.2.3 Ultrafiltration

Ultrafiltration has been lab studied since 1907. Ultrafiltration membranes do not generate any significant osmotic pressure due to their porous structure. Ultrafiltration membrane pores range in size from five to one hundred nanometers and operate at pressures less than one MPa. Due to their pore structure, ultrafiltration membranes allow for the permeability of micro-solutes with molecular weights less than 300 Da. Typically, ultrafiltration membranes are used as a pretreatment to nanofiltration or reverse osmosis to separate out macromolecules, colloids, and solutes with molecular weights greater than 10,000 Daltons [1].

1.2.4 Microfiltration

Microfiltration membranes have relatively large pores (0.1 to 10 microns in size) and operate at low applied pressures of five to five hundred kPa. Microfiltration membranes have limited use in desalination methods due to their pore size. Microfiltration membranes are typically used to separate out viruses and bacteria. Applications of microfiltration in water treatment more broadly increased popularity after the cryptosporidium outbreak in 1992 in Milwaukee, WI [1].

1.3 Covalent Organic Framework (COF) Membranes

Covalent Organic Frameworks (COFs) are a novel class of porous crystalline materials that are considered a breakthrough in membrane technology, among other applications. COFs are low density materials that can be constructed by different organic linkers of varying structures via strong covalent bonds. These strong bonds create materials with predictable crystalline structures [17, 18].

Recently, COF membranes have gained interest as a potential desalination tool. For example, Lin, et al. reported salt rejection of at least 91% for various covalent triazine framework (CTF) membranes, which are a subset of COFs [19]. Additionally, Zhang, et al. reported a salt

rejection of over 98% for computationally designed TpPa-x COF membranes of various functional groups [20].

1.4 Membrane Fouling

Membrane fouling is the primary issue plaguing membrane systems. Fouling negatively affects the quality and quantity of treated water passing through the membrane and reduces permeate flux over time [11, 13, 14]. Because of this, fouling prevention and remediation are areas of interest for researchers. Membrane fouling takes many forms, but broadly, it is defined as a phenomenon wherein flow through the membrane is hindered by the accumulation of undesired deposits on the membrane's surface, or in the membrane's pores [1, 11, 21]. Fouling is a particularly complex research topic because there are so many variables that determine what fouling will look like and how foulants will behave in a membrane system. There are several different categories of foulants, different fouling mechanisms, different cleaning processes that work in different scenarios and under different conditions, etc. This section will cover some of the core complexities researchers are facing regarding this topic.

Membrane systems can operate in one of two ways: constant permeate flux (flow rate per unit membrane area) with variable transmembrane pressure, or constant pressure with variable permeate flux. The latter is more common and simpler to operate [11].

One primary complexity with membrane fouling is the variety of different foulants that can be seen. Particulates are inorganic or organic particles or colloids that physically "blind" the membrane surface and block pores or develop a cake layer. Particulates act as foulants by hindering transport to the membrane surface. Organic foulants are dissolved components and colloids (e.g., humic and fulvic acids, proteins, polysaccharides, etc.) which tend to attach to the membrane by adsorption. Inorganic foulants consist of dissolved inorganic components (e.g., iron, manganese,

silica) which precipitate onto the membrane surface after a pH change (i.e., scaling) or due to oxidation (i.e., iron oxides and manganese oxides). Residuals from coagulants and flocculants can also be present in waters and can act as inorganic foulants. Biological foulants consist of vegetative matter (such as algae) or microorganisms (such as bacteria) which tend to adhere to membranes and cause biofilm formation (also referred to as bio-fouling) [11, 22].

Fouling is caused by a wide array of complex chemical and physical interactions, making research on fouling prevention difficult. The characteristics of foulants are determined by several factors, including the feed water composition, the concentration of the various constituents, the water chemistry, the membrane properties, temperature, the mode of operation, and the hydrodynamic conditions [11].

Broadly, membrane fouling can be described by four different fundamental mechanisms: complete blocking, intermediate blocking, standard blocking, and cake filtration. Complete blocking describes a fouling mode wherein the foulant particles completely seal off the membrane's pores and prevent flow. Intermediate fouling describes a similar phenomenon, however only a portion of the particles seal off the membrane's pores, and the remainder of the particles accumulate on top of other deposited particles. During standard blocking, instead of particles accumulating on top of the membrane surface, the particles accumulate on the walls of the pores which are assumed to be straight and perfectly cylindrical. As particles accumulate within the pores, the pore diameters decrease, which reduces the membrane's permeability. Cake filtration describes a scenario in which the foulant accumulates on top of the membrane surface, creating a permeable cake layer that increases in thickness as more particles deposit [23, 24, 25]. These single fouling mechanisms have established mathematical models, published by Hermia in 1982 (Table

1) [25]. However, often in experimental and real-world scenarios, multiple fouling mechanisms are at play.

Table 1 Constant-pressure single fouling models [24, 25].

Model	**Equation**	**Fitted Parameters**
Complete blocking	$V = \frac{J_0}{K_b}(1 - e^{K_b t})$ (4)	K_b (s^{-1})
Intermediate blocking	$V = \frac{1}{K_i}\ln(1 + K_i J_0 t)$ (5)	K_i (m^{-1})
Standard blocking	$V = (\frac{1}{J_0 t} + \frac{K_s}{2})^{-1}$ (3)**Error! Reference source not found.**	K_s (m^{-1})
Cake filtration	$V = \frac{1}{K_c J_0}(\sqrt{1 + 2K_c {J_0}^2 t} - 1)$ (6)	K_c (s/m^2)

Bolton, et al combined the four single fouling models summarized in Table 1 to derive five combined fouling models to describe these multi-mechanism scenarios. Cake filtration and complete blocking are combined to create a "cake-complete" model, cake filtration and intermediate blocking are combined to create a "cake-intermediate" model, complete and standard blocking are combined to create a "complete-standard" model, intermediate and standard blocking are combined to create an "intermediate-standard" model, and cake filtration is combined with standard blocking to create a "cake-standard" model (Table 2) [24].

Table 2 Constant-pressure combined fouling models [24].

Model	Equation	Fitted Parameters
Cake-complete	$V = \frac{J_0}{K_b}(1 - e^{\frac{-K_b}{K_c {J_0}^2}(\sqrt{1+2K_c {J_0}^2 t}-1)})$ (9)	K_c (s/m^2), K_b (s^{-1})
Cake-intermediate	$V = \frac{1}{K_i}\ln(1 + \frac{K_i}{K_c J_0}(\sqrt{1 + 2K_c {J_0}^2 t} - 1))$ (7)	K_c (s/m^2), K_i (m^{-1})
Compete-standard	$V = \frac{J_0}{K_b}(1 - e^{\frac{-2K_b t}{2+K_s J_0 t}})$ (10)	K_b (s^{-1}), K_s (m^{-1})
Intermediate-standard	$V = \frac{1}{K_i}\ln(1 + \frac{2K_i t}{2+K_s J_0 t})$ (8)	K_i (m^{-1}), K_s (m^{-1})
Cake-standard	$V = \frac{2}{K_s}\left(\beta\cos\left(\frac{2\pi}{3} - \frac{1}{3}\cos^{-1}(\alpha)\right) + \frac{1}{3}\right)$, $\alpha = \frac{8}{27\beta^3} + \frac{4K_s}{3\beta^3 K_c J_0} - \frac{4{K_s}^2 t}{3\beta^3 K_c}$, $\beta = \sqrt{\frac{4}{9} + \frac{4K_s}{3K_c J_0} + \frac{2{K_s}^2 t}{3K_c}}$ (11)	K_c (s/m^2), K_s (m^{-1})

The deposition of foulants onto the surface or into the pores of a membrane is thought to be governed by the interaction and hydrodynamic drag forces experienced by the foulant. The foulant experiences membrane-foulant and foulant-foulant interaction forces, as well as drag [26]. It is hypothesized that a membrane system will have a critical flux below which fouling, and thus flux decline, should be insignificant. Essentially, there may be some "limiting value" or pseudo-stable flux for which a membrane system exceeding that value will eventually decline to that limiting flux. Additionally, assuming the deposition of foulants is governed by the hydrodynamic drag and interaction forces experienced by the foulant, the limiting flux would then likewise be determined by those forces. In this case, the limiting flux would be assumed to be independent of the initial flux. Limiting flux is an important topic of research in membrane filtration because if a

limiting flux can be determined, then operation at or below that flux could lead to minimal fouling and flux decline over time [27, 28].

1.5 Membrane Cleaning

Fouling is inevitable in membrane use; thus, cleaning is a necessary process in healthy and sustainable membrane system operations. Five common categories of chemical cleaning agents are typically considered for membrane cleaning: alkalines, acids, metal chelating agents, surfactants, and enzymes. Chemical cleaning agents clean a membrane by either removing the foulant, changing the morphology of the foulant, or altering the fouling layer surface chemistry [29].

Fouling can be classified as reversible or irreversible. Reversible fouling occurs due to a cake layer or material concentration polarization at the membrane surface. Reversible fouling can be backwashable (able to be restored through physical washing) or non-backwashable (able to be restored only by chemical cleaning). Irreversible fouling occurs due to chemisorption and pore plugging. When irreversible fouling occurs, the membrane must either go through extensive chemical cleaning or be replaced [11, 30].

In a 2004 study, several chemical cleaning agents were compared for their effects on organic foulants on nanofiltration membranes. The cleaning solutions studied included DI water (baseline), NaOH with a pH of 11 for an alkaline solution, certified grade sodium ethylenediaminetetraacetate (EDTA) at a molarity of one mM as a metal chelating agent, and certified grade sodium dodecyl sulfate (SDS) at molarities of one, five, ten, and thirty-five mM as anionic surfactants. The nanofiltration membrane used was negatively charged and smooth. The feed solution was Suwanee River humic acid (SRHA) at pH 8.1 with varying added cations (magnesium, calcium, and sodium) [29].

The study found that all cleaning solutions, even DI water, worked well and saw the flux was fully recovered for samples fouled with feedwater solutions containing calcium ions. However, when magnesium and sodium ions were present, DI water and NaOH were ineffective. EDTA and SDS cleaning recovered the initial flux for all feedwater solutions. It was found that the efficacy of EDTA cleaning was highly dependent on solution pH, whereas pH had little to no effect on SDS cleaning. Additionally, recovered flux increased with increasing SDS molar concentration. Finally, the effect of cleaning on the forces present in membrane fouling layers was discussed. During chemical cleaning, the foulant inside the fouling layer experiences two types of forces: adhesion forces, and shearing forces. The addition of cleaning solutions was found to drastically reduce the adhesion forces. EDTA and SDS cleaning eliminated the adhesion forces entirely. However, significant adhesion forces were still present after NaOH cleaning. This study provides much needed reference data regarding fouling behavior and how chemical cleaning affects organic fouling layers on nanofiltration membranes, and membranes in general [29].

Different fouling methods and membrane system conditions create a complex fouling environment with many variables to consider. Once fouling occurs, it reduces the permeate flux, increases the feed pressure, reduces system productivity, increases maintenance and operation costs from membrane cleaning, and decreases membrane lifespan [29]. Additional research into fouling prevention and membrane cleaning can reduce all these concerns and increase the cost effectiveness of pressure-driven desalination techniques.

1.6 Goals and Objectives

The goal of this study is to compare the fouling behavior and mechanisms of a new membrane technology – a lab-synthesized COF nanofiltration membrane – with a well-researched and established commercial – a DuPont NF270 nanofiltration membrane – in a high concentration

organic fouling scenario at various pressures. While the pressure and membrane will vary by experimental run, foulant concentration, feedwater chemistry, and flow rate will remain constant throughout. There are several objectives for the analysis of these experiments. Analyses will be conducted of the average fouling rate, single and combined fouling mechanisms via mathematical models, and limiting flux.

1.7 Organization

In chapter 1, a review of the literature and policies on pressure-driven membrane systems and desalination was conducted. Additionally, research goals and objectives for this study were provided. Chapter 2 will cover the materials and experimental methodology. In chapter 3, the experimental results will be discussed. The analyses conducted for this study include: an analysis of the flux data over the course of the experiments, average fouling rates, mathematical models of fouling mechanisms, and limiting flux. Finally, chapter 4 will consist of the study's conclusion, as well as recommendations for future work.

Chapter 2: Materials and Methodology

2.1 Overview

Membrane fouling is the key concern limiting membrane water filtration technology. Membrane fouling causes the membrane's permeate flux to decrease over time, reduces the membrane's lifespan, and increases water treatment energy requirements. Membrane fouling prevention or reduction is key to reducing the cost of membrane water treatment processes. This experiment explores differences in fouling behavior and fouling mechanisms between two nanofiltration membranes: commercial NF270 membranes and internally synthesized COF membranes.

Generally, membrane fouling experiments consists of three to four main processes: compaction, conditioning, fouling, and sometimes cleaning [14, 27-30]. Compaction refers to a process in which pure de-ionized (DI) water is run through the membrane for a period of time in order to reach a stabilized flux and compact the membrane as a way to prime it for filtration. This is a necessary process in order to maintain consistent results later in the fouling process. Conditioning is a process similar to compaction, but instead of pure DI water, a foulant-free electrolyte solution is used. This process is meant to "condition" the membrane, stabilize the experimental conditions, and reach a baseline prior to the foulant's introduction. Fouling refers to the main experiment when the foulant solution is run through the membrane for a period of time in which the flux and/or the pressure maintained by the membrane is tracked. Finally, an experiment may include one or more post-fouling cleaning processes to attempt to regain the lost flux, but that is beyond the scope of this chapter. The parameters (time, pressure, etc.) set during the compaction and conditioning processes are critically important. The membrane must be

properly compacted and primed in order to ensure accurate measurements and results during the fouling period.

Yi-Ning Wang, et al [31] perform a relevant organic fouling study. The experiment begins with a 2-day (48 hour) compaction process with pure DI water using the same pressure used in the fouling process. The pressure differed based on the desired initial flux. There was no foulant-free conditioning. In the fouling experiment, proteins bovine serum albumin (BSA) and lysozyme were tested at 20 mg/L at a constant pressure, with initial fluxes or either 75 LMH or 120 LMH. Fouling solutions of ionic strengths 10 mM and 100 mM were tested. Tang, et al [32] performed a similar organic fouling experiment. In this trial, the authors begin with a 2-day (48-hour) compaction process using the same pressure to be used in the fouling process (200 psi). After compaction, a 1-day (24-hour) conditioning process was performed, again at 200 psi. Finally, the fouling experiment tested a foulant solution of 5 mg/L pre-treated Aldrich humic acid (PAHA) at an ionic strength of 10 mM with a constant pressure of 200 psi. Li, et al [29] performed another organic fouling experiment. In this experiment, DI water compaction was performed at 120 psi for a nondescript amount of time. Per the article, the compaction was performed "until flux had stabilized." Secondly, before the foulant was introduced, a foulant-free conditioning process was performed at 120 psi for 2 hours. The foulant solution consisted of 1 g/L Suwanee River humic acid (SRHA) which was tested at a constant flux (as opposed to constant pressure) of 18.0 μm/s.

In the literature, there is a wide range of times and pressures used for compaction and conditioning processes. The goal of methodological optimization is to reduce research resources necessary for completing these experiments, as well as to increase the reliability of data output. In general, higher operating pressure and longer timeframes increase the likelihood that the compaction and conditioning processes have adequately primed the membrane. A timeframe of 24

to 48 hours for compaction and/or conditioning is at the high end of what is seen in the literature and thus is likely to sufficiently prime the membrane for fouling.

This analysis will explore the organic fouling behaviors and mechanisms in nanofiltration membranes at varying constant pressure, constant flow scenarios using a high-concentration sodium alginate solution. The experiments were run using constant pressure and constant flow to mimic real world scenarios in water treatment processes. Additionally, because the fouling period will only be 24-hours, a high-concentration foulant solution was used to better simulate how a lower concentration foulant may act over a longer period of time in a real-world scenario.

2.2 Materials

This experiment utilized commercially manufactured DuPont NF-270 nanofiltration membranes and Covalent Organic Framework (COF) TpHz membranes which were synthesized by the University of Wisconsin – Milwaukee's Department of Material Science. Both types of membranes were tested under the same experimental parameters, as discussed below.

The membranes were soaked in DI water for a minimum of 24-hours prior to testing. For initial compaction, pure DI water was used. The foulant-free conditioning was an electrolyte solution of 7 mM sodium chloride and 1 mM calcium chloride (10 mM total ionic strength) with a neutral pH of 7.0 +0.0/-0.1. The organic fouling solution was a brown algae-based polysaccharide solution of 500 milligram per liter sodium alginate with 7 mM sodium chloride and 1 mM calcium chloride (10 mM total ionic strength) at a neutral pH of 7.0 +0.0/-0.1.

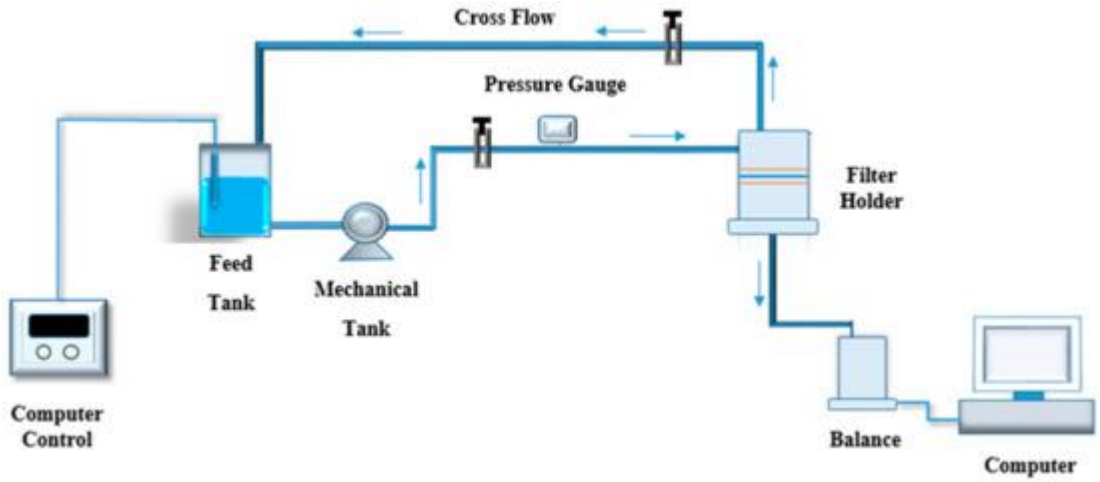

Figure 3 Schematic of cross-flow membrane filtration system [33].

The experimental setup consisted of a commercial Aquatec CDP 8800 pump, tubing, a membrane cell, two pressure gages, two fluid valves, and a flow rate gage. Figure 3 shows a schematic view of the experimental setup. A beaker was set on an electronic scale below the outflow point of the membrane cell to measure the mass of the permeate throughout the experiment in order to calculate the flux (1) and permeance (2).

2.3 Experimental Methodology

Membranes were compacted at a constant pressure of 80 psi for 24 hours with pure DI water. Due to laboratory limitations, 80 psi is the highest stable pressure able to be reached, thus a minimum of 24-hours was allotted for optimal compaction.

Following compaction, membranes were processed through a conditioning baseline using a foulant-free electrolyte solution of 7 mM sodium chloride and 1 mM calcium chloride (10 mM total ionic strength). The conditioning process was performed at two to three different constant pressure environments at either 40, 60, or 80 psi for NF270, and 60 or 80 psi for COF for 24 hours.

After the conditioning process, the foulant was added. During the fouling processes, membranes were run with a polysaccharide solution of 500 milligrams per liter sodium alginate

solution with 7 mM sodium chloride and 1 mM calcium chloride (10 mM total ionic strength) at the same pressure as experienced during the conditioning process: 40, 60, or 80 psi for 24 hours. The total experiment runtime was 72 hours per membrane, with 24 hours for each process (compaction, conditioning, and organic fouling) running consecutively.

The flow rate was held constant at 0.225 ± 0.025 liters per minute, and the temperature was held at room temperature (20 degrees Celsius) for all processes in all experiments.

Two control tests were conducted using COF TpHz nanofiltration membranes. The first control test consisted of 24-hours of DI water compaction at a constant pressure of 80 psi, followed by 48 hours of foulant-free conditioning at a constant pressure of 80 psi using a solution of 7 mM sodium chloride, 1 mM calcium chloride (10 mM total ionic strength) with no addition of a foulant. The second control test consisted of 24-hours of DI water compaction at a constant pressure of 80 psi, followed by 48 hours of foulant-free conditioning at a constant pressure of 60 psi using a solution of 7 mM sodium chloride, 1 mM calcium chloride (10 mM total ionic strength) with no addition of a foulant. All control tests were held at a constant flow rate of 0.225 ± 0.025 liters per minute.

Throughout the experiment, mass measurements of the permeate dispensed through the membrane were taken and recorded. With these mass measurements, the instantaneous flux (1) and permeance (2) were calculated.

$$flux = m * \frac{1\ L\ H_2O}{1000\ g\ H_2O} \quad (1)$$

$$permeance = m * \frac{1\ L\ H_2O}{1000\ g\ H_2O} * \frac{1}{A_S * P * t} = \frac{flux}{P} \quad (2)$$

Wherein,

m = mass of permeate (g);

A_s = membrane surface area (m^2);

t = time (hour);

P = pressure (bar).

Chapter 3: Results and Discussion

A visible thick gel-like layer was observed on the membrane surfaces after 24-hours of fouling with the 500 milligrams per liter sodium alginate solution. If this observed foulant layer is a cake layer, the primary fouling mechanism will likely be cake filtration (Figures 8-10).

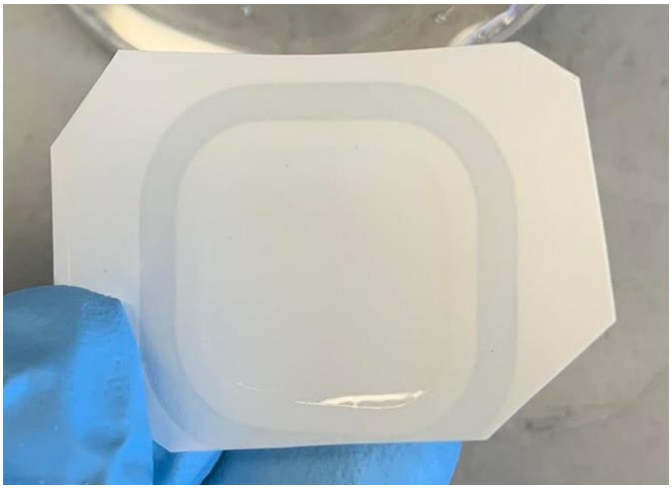

Figure 4 NF270 Membrane after 24-hours organic fouling with 500 mg/L sodium alginate. Note that because the membrane is white, the foulant layer is not very visible via digital photo. Reference Figure 5 for a better representation of the fouling layer.

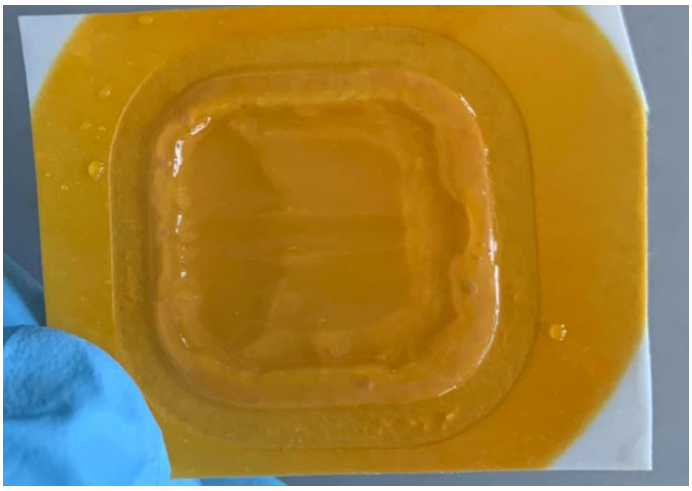

Figure 5 COF membrane after 24-hours of organic fouling with 500 mg/L sodium alginate.

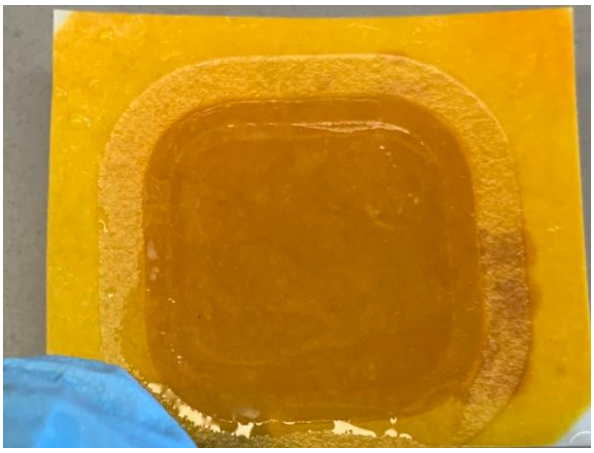

Figure 6 Control COF membrane. No foulant added.

3.1 Organic fouling in NF-270 membranes

The calculated flux was normalized by the initial flux in Figure 11. Slight flux decline is observed during DI-water compaction, followed by a stable flux during foulant-free conditioning. A significant flux decline is observed during the first several minutes of organic fouling, followed by a slow decline toward a near-constant quasi-steady flux. Figures 12-14 show the flux over time during the final 24 hours of the experiment, consisting of the organic fouling period.

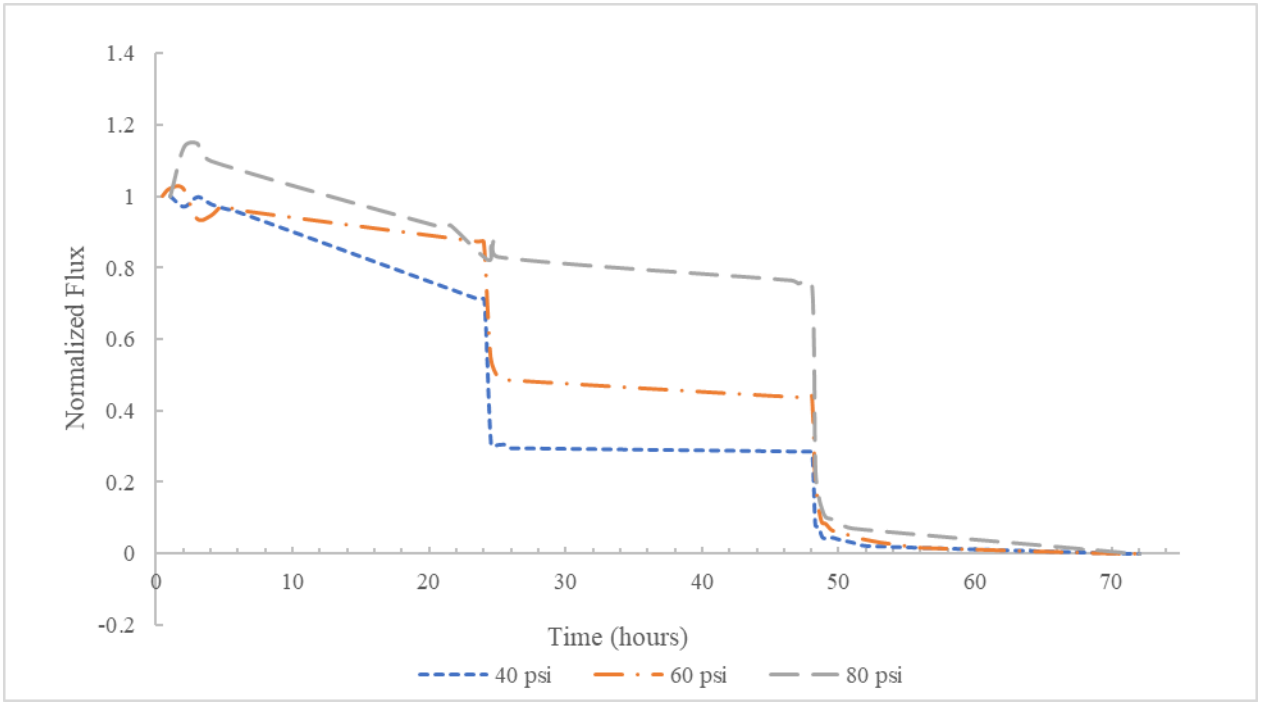

Figure 7 Change in flux over time during full 72-hour experiment consisting of DI Water Compaction, Foulant-free Conditioning, and Organic Fouling in NF270 membranes at 40 psi, 60 psi, and 80 psi.

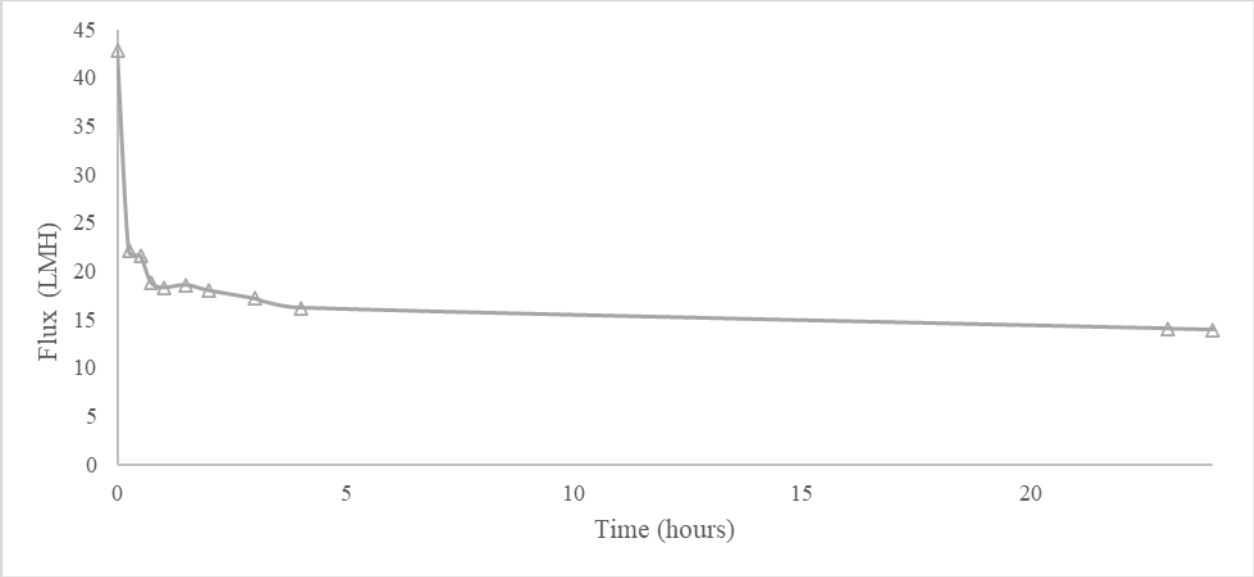

Figure 8 Change in flux over time, normalized by initial flux, during organic fouling by 500 mg/L sodium alginate in DuPont NF-270 membranes at a constant pressure of 40 psi

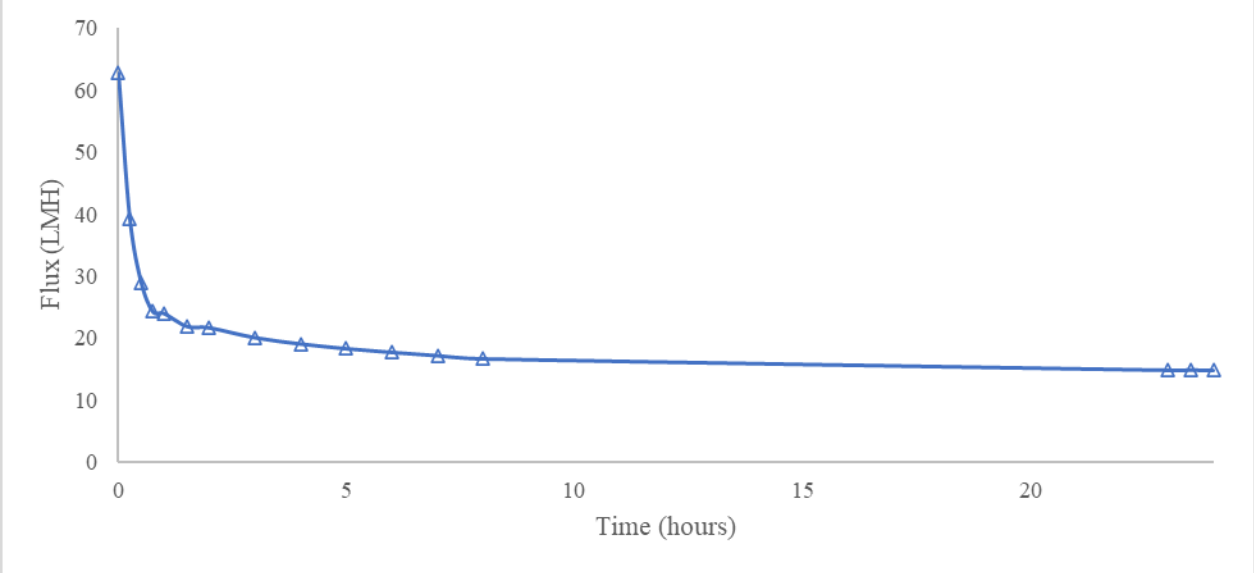

Figure 9 Change in flux over time, normalized by initial flux, during organic fouling by 500 mg/L sodium alginate in DuPont NF-270 membranes at a constant pressure of 60 psi over a 24-hour period.

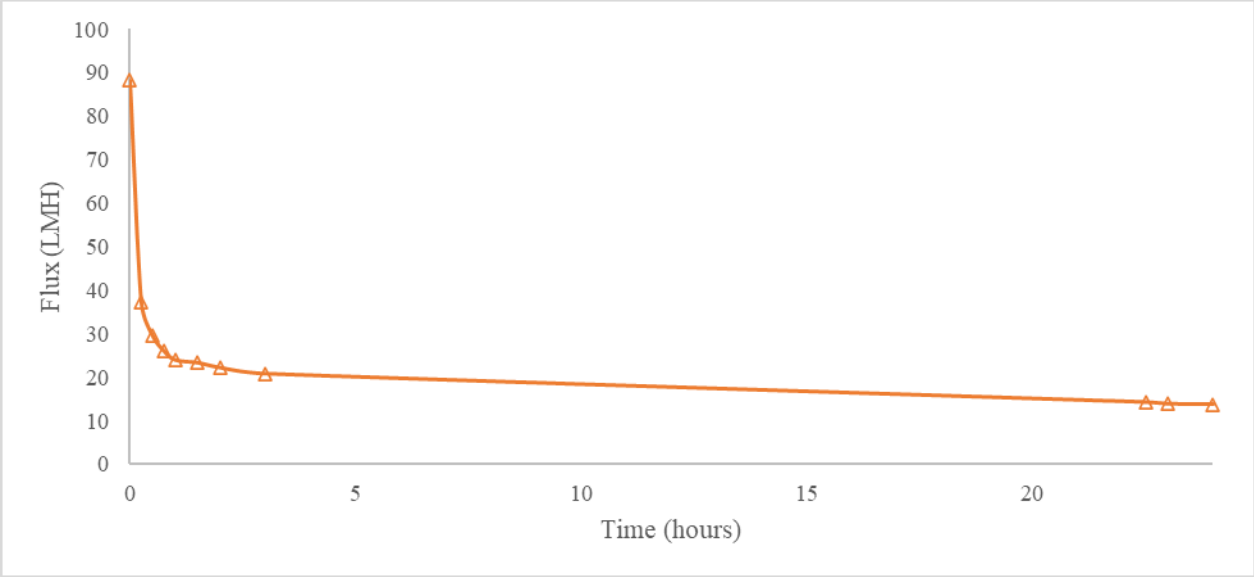

Figure 10 Change in flux over time, normalized by initial flux, during organic fouling by 500 mg/L sodium alginate in DuPont NF-270 membranes at a constant pressure of 80 psi over a 24-hour period.

3.2 Organic Fouling in COF membranes

The calculated flux was normalized by the initial flux in Figure 15. Flux decline is observed during DI-water compaction, followed by a stable flux during foulant-free conditioning. A significant flux decline is observed during the first several minutes of organic fouling, followed by a slow decline toward a near-constant quasi-steady flux. Figures 16-17 show the flux over time during the final 24 hours of the experiment, consisting of the organic fouling period.

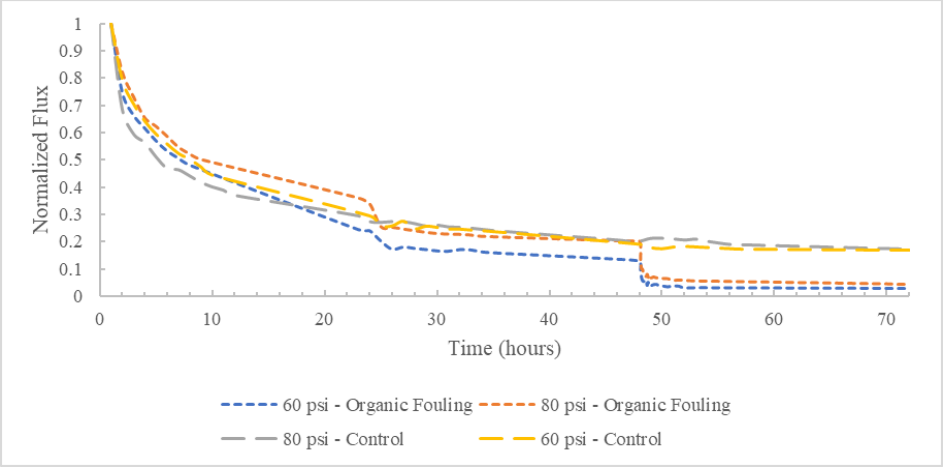

Figure 11 Change in flux over time during full 72-hour experiment consisting of DI-Water Compaction, Foulant-free Conditioning, and Organic Fouling in COF membranes at 60 psi and 80 psi.

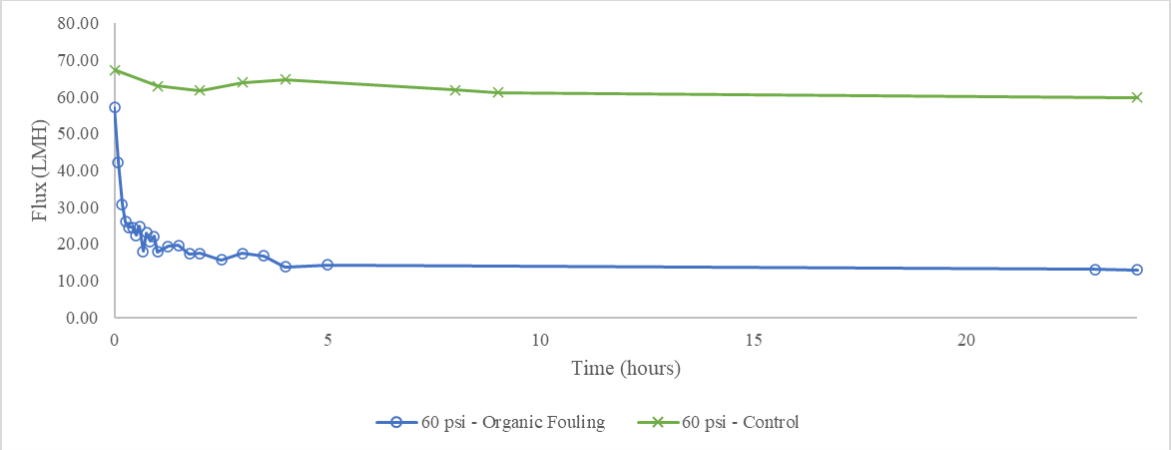

Figure 12 Change in flux over time during organic fouling by 500 mg/L sodium alginate in TpHz COF membrane at constant pressures of 60 psi over a 24-hour period compared to the control.

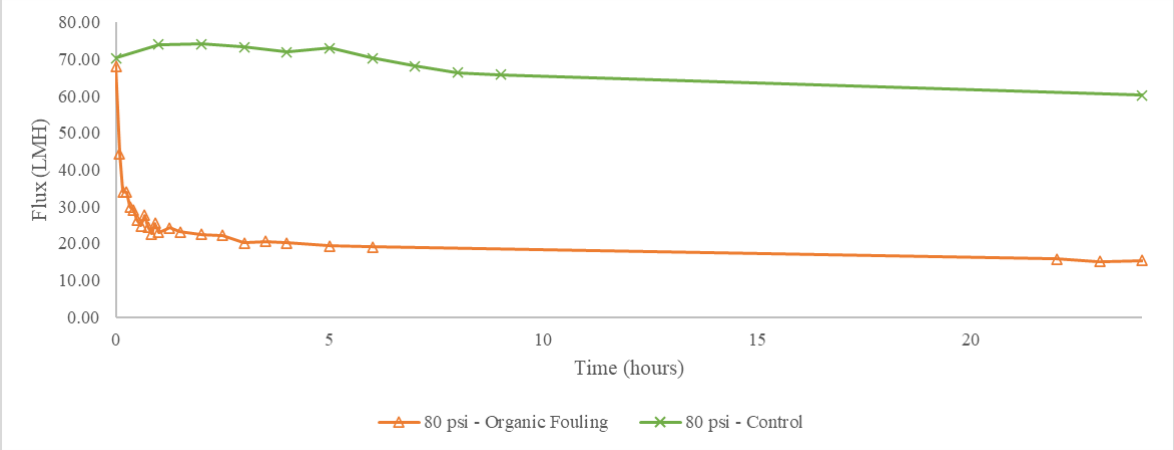

Figure 13 Change in flux over time during organic fouling by 500 mg/L sodium alginate in TpHz COF membrane at constant pressures of 80 psi over a 24-hour period compared to the control.

3.3 Fouling Rate

Fouling rate is the rate at which a membrane's permeate flux declines over time. Simply, the average fouling rate over a period of time can be estimated by taking the absolute value of the slope of a linear regression model fit to the flux versus time curve during the fouling period of the experiment. Referencing Figures 12-14, 16 and 17, a sharp decline in the flux can be seen over the initial 15 minutes of the experiment, followed by a slow decline to a quasi-steady flux by the end of the 24-hour fouling period. These two distinct stages (hours 0 to 0.25, and hours 0.25 to 24) can be separated in order to find two separate fouling rates for the two separate stages. NF270 and

COF membrane experiments conducted at constant pressures of 60 and 80 psi are evaluated in this section in order to compare the fouling rate behavior between the two membranes as well as between the two pressures.

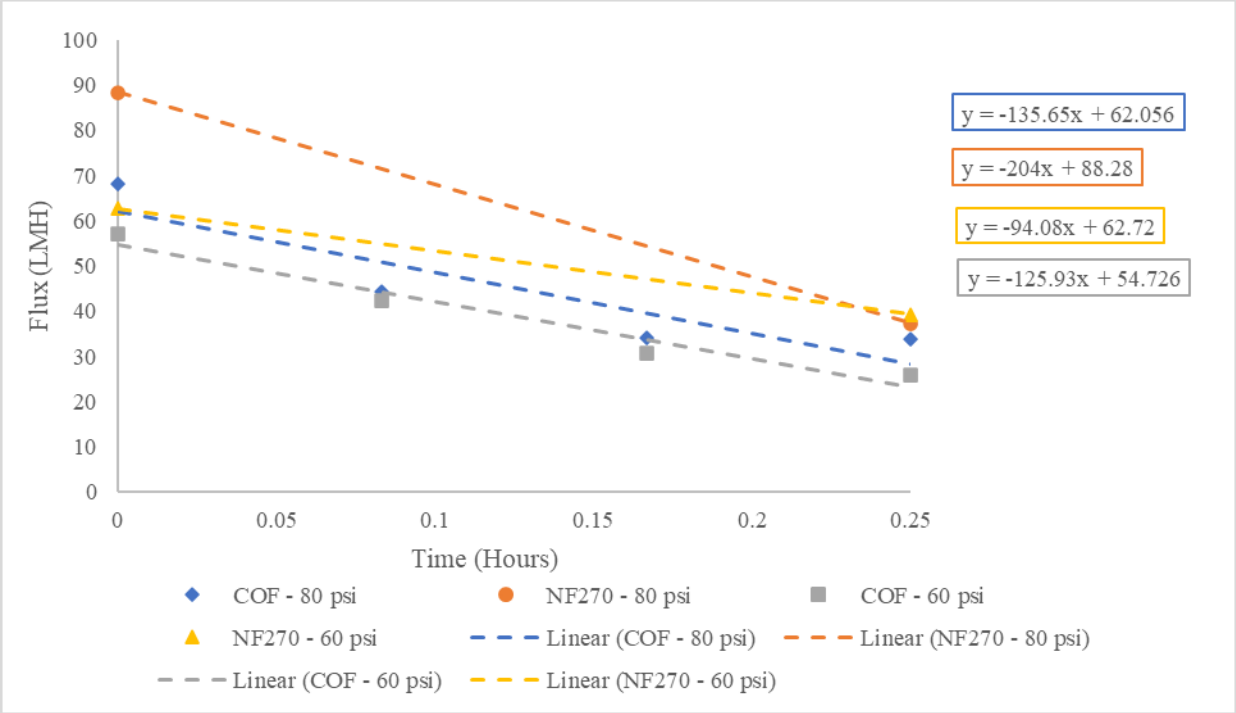

Figure 14 Flux versus time during Stage 1 (first fifteen minutes) of the organic fouling period of NF270 and COF membranes at 60 and 80 psi. Linear regression lines are fit to each dataset. The slope of each linear regression is equal to the average change in flux over the given time period. The absolute value of the slope can be used as an estimated flux decline for the initial fouling period.

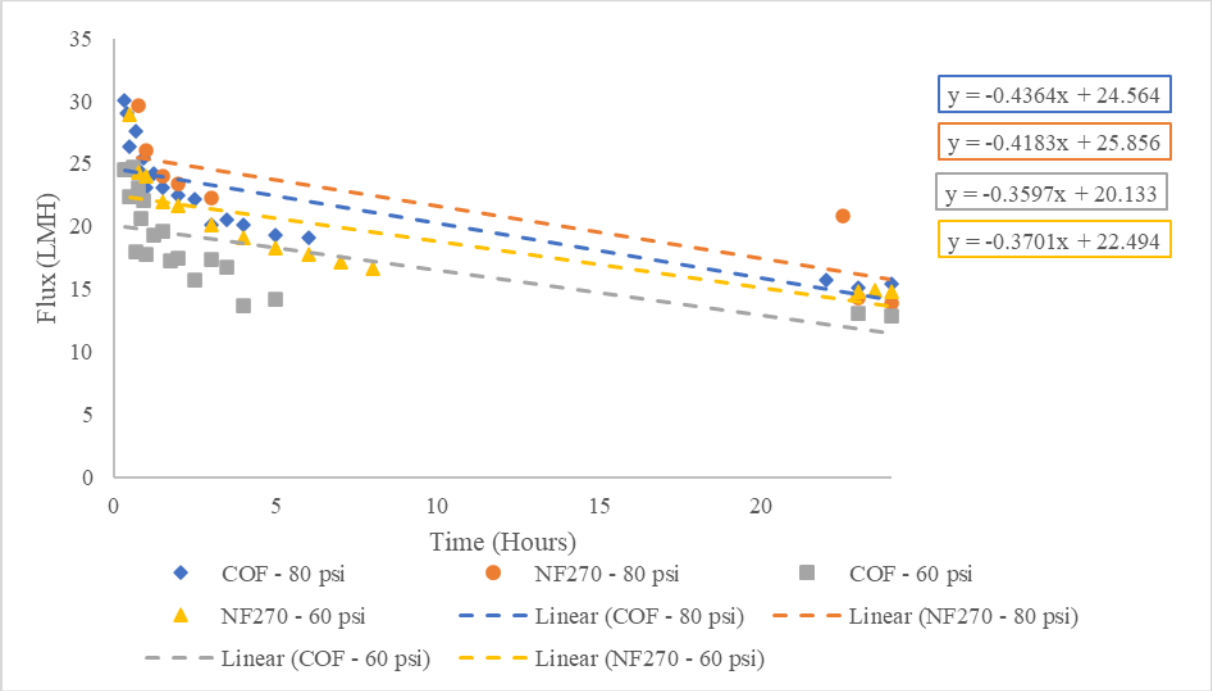

Figure 15 Flux versus time during Stage 2 (final twenty-three hours and forty-five minutes) of the organic fouling period of NF270 and COF membranes at 60 and 80 psi. Linear regression lines are fit to each dataset. The slope of each linear regression is equal to the average change in flux over the given time period. The absolute value of the slope can be used as an estimated flux decline for the final fouling period.

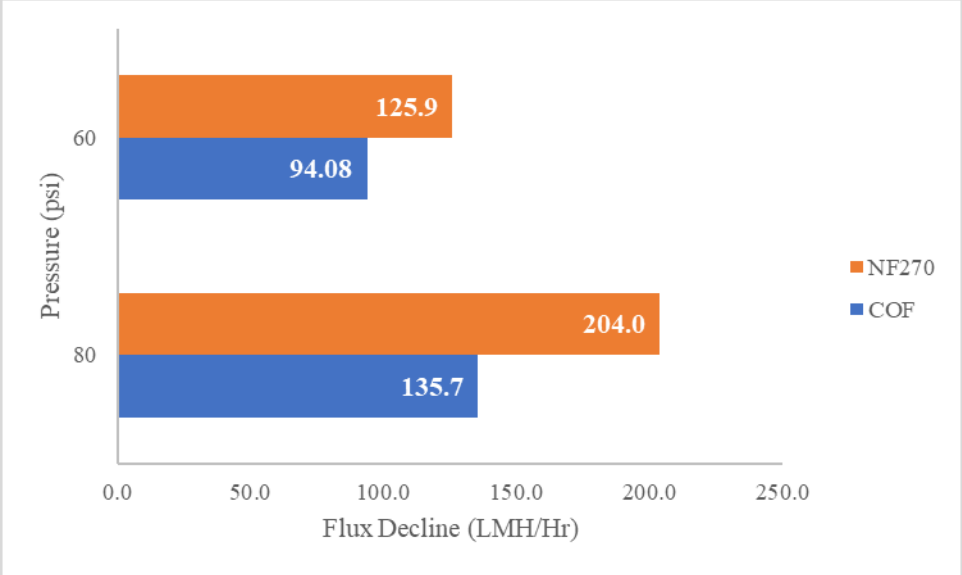

Figure 16 Flux decline versus pressure during Stage 1 (first fifteen minutes) of the organic fouling period of NF270 and COF membranes at 60 and 80 psi.

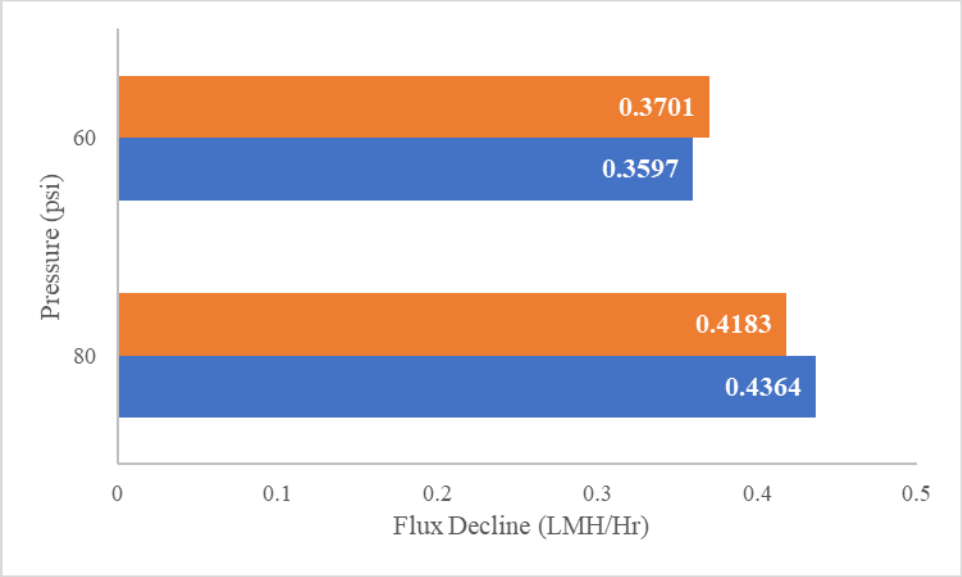

Figure 17 Flux decline versus pressure during Stage 2 (final twenty-three hours and forty-five minutes) of the organic fouling period of NF270 and COF membranes at 60 and 80 psi.

Stage 1 is defined as the first 15 minutes (hours 0 through 0.25) of the fouling period. The vast majority of the flux decline occurs during this stage. The NF270 membranes see flux declines during the 60 psi and 80 psi experiments of 1.259×10^{2} LMH/hour and 2.040×10^{2} LMH/hour, respectively, during this stage. The COF membranes see flux declines during 60 psi and 80 psi experiments of 9.408×10^{1} LMH/hour and 1.357×10^{2} LMH/hour, respectively, during this stage. With both membranes, an increase in the stage 1 fouling rate is observed with increasing pressure (Figure 14 and Figure 16).

Stage 2 is defined as the final 23.75 hours of the fouling period. Relatively little change is seen in the flux during this stage. A quasi-steady rate has already been achieved after the initial fouling period (stage 1). The NF270 membranes see flux declines during the 60 psi and 80 psi experiments of 3.701×10^{-1} LMH/hour and 4.183×10^{-1} LMH/hour, respectively, during this stage. The COF membranes see flux declines during 60 psi and 80 psi experiments of 3.957×10^{-1} LMH/hour and 4.364×10^{-1} LMH/hour, respectively, during this stage. Despite the relatively low

flux decline during this stage, an increase in the stage 2 fouling rate is observed with increasing pressure with both membranes, similar to stage 1 (Figure 15 and Figure 17).

The increase in fouling rates with respect to increasing pressure is expected. With increasing pressure, foulant particles have a greater opportunity to deposit and/or accumulate on or within the membrane, which is expected to speed up the fouling process, as was observed in this experiment. During stage 1, the fouling rate is higher in both pressure systems with the commercial NF270 membranes than with the lab-synthesized COF membranes. More experiments are needed to determine a specific numerical relationship. No significant difference was seen between the two types of membranes in stage 2.

3.4 Fouling Mechanism Modelling

Fouling mechanisms in constant flow scenarios were mathematically modeled by Hermia [25] and adapted by Bolton, et al [24] into combined models (Table 1, Table 2). In real-world and experimental scenarios, often multiple fouling mechanisms are at play. Single fouling models are a useful tool for finding the primary fouling mechanism [25]. However, using combined fouling models rather than single fouling models, a better understanding of the mechanisms being observed and how they interact can be found. Single and combined mechanism modeling was performed to compare with the experimental data from the NF270 and COF membranes at in constant pressure environments of 60 psi and 80 psi. In all cases, model fit error was calculated as SSR (sum squared residuals or sum squared regression) and model fit variance was calculated as the R^2 value. It was hypothesized that cake filtration would be a primary fouling mechanism because sodium alginate has a gelatinizing quality that may be susceptible to building a cake layer, and because when the experiments were completed, all membranes were left with a visible thick gel-like layer on the membrane surface (Figure 4 and Figure 5).

3.4.1 Nomenclature

J_0 = Initial flux (LMH);

K_b = Complete blocking constant ($hour^{-1}$);

K_c = Cake filtration constant ($hour/m^2$);

K_i = Intermediate blocking constant (m^{-1});

K_s = Standard blocking constant (m^{-1});

t = time (hours);

V = volume of permeate (L).

3.4.2 Single Fouling Models

$$V = \left(\frac{1}{J_0 t} + \frac{K_s}{2}\right)^{-1} \quad (3)$$

The standard blocking model (3) is a single fouling model describing foulant deposits accumulating entirely inside the membrane's pores. For the COF membrane experiments at 80 psi and 60 psi, the model fit error was 2.425×10^{-1} and 1.475×10^{-1}, respectively, and the R^2 values were 0.0142 and 0.0149. For the NF270 membrane experiments at 80 psi and 60 psi, the model fit error was 1.914×10^{-1} and 2.137×10^{-1}, respectively, and the R^2 values were 0.0149 and 0.0149 (Table 3).

$$V = \frac{J_0}{K_b}\left(1 - e^{K_b t}\right) \quad (4)$$

The complete blocking model (4) is a single fouling model describing foulant deposits accumulating entirely on the membrane's surface. For the COF membrane experiments at 80 psi and 60 psi, the model fit error was 2.427×10^{-1} and 1.477×10^{-1}, respectively, and the R^2 values were 0.0131 and 0.0138. For the NF270 membrane experiments at 80 psi and 60 psi, the model fit error was 1.916×10^{-1} and 2.139×10^{-1}, respectively, and the R^2 values were 0.0139 and 0.0136 (Table 3).

$$V = \frac{1}{K_i} ln(1 + K_i J_0 t) \quad (5)$$

The intermediate blocking model (5) is a single fouling model describing a fouling mechanism wherein the foulant deposits partially within the membrane pores, and partially on top of the membrane surface. For the COF membrane experiments at 80 psi and 60 psi, the model fit error was 1.772×10^{-1} and 1.069×10^{-1}, respectively, and the R^2 values were 0.2796 and 0.2862. For the NF270 membrane experiments at 80 psi and 60 psi, the model fit error was $1.386\ 10^{-1}$ and 1.534×10^{-1}, respectively, and the R^2 values were 0.2865 and 0.2884 (Table 3).

$$V = \frac{1}{K_c J_0} (\sqrt{1 + 2K_c {J_0}^2 t} - 1) \quad (6)$$

The cake filtration model (6) is a single fouling model describing a fouling mechanism wherein a cake layer of increasing size is formed. For the COF membrane experiments at 80 psi and 60 psi, the model fit error was 2.422×10^{-2} and 1.312×10^{-2}, respectively, and the R^2 values were 0.9016 and 0.9124. For the NF270 membrane experiments at 80 psi and 60 psi, the model fit error was 1.667×10^{-2} and 1.957×10^{-2}, respectively, and the R^2 values were 0.9142 and 0.9098 (Table 3).

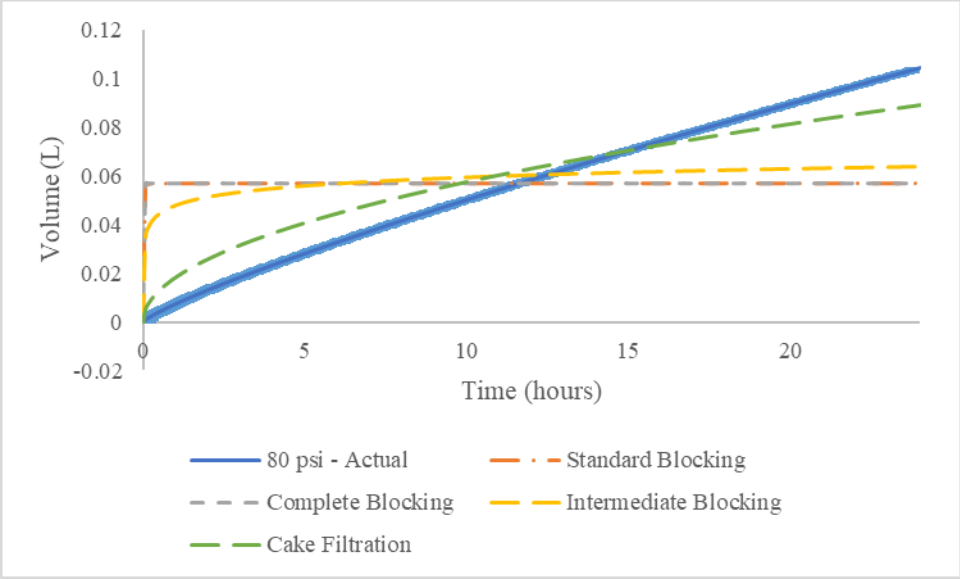

Figure 18 Volume versus time of COF membrane fouled for 24-hours with 500 mg/L of sodium alginate at a constant pressure of 80 psi compared to Standard Blocking, Complete Blocking, Intermediate Blocking, and Cake Filtration models. Data is the average of two runs with error bars of standard error.

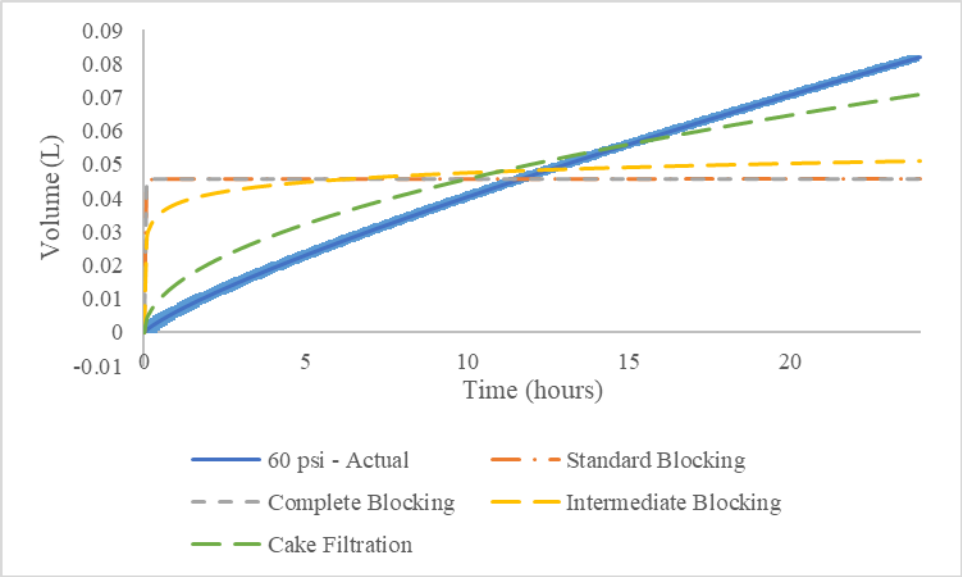

Figure 19 Volume versus time of COF membrane fouled for 24-hours with 500 mg/L of sodium alginate at a constant pressure of 60 psi compared to Standard Blocking, Complete Blocking, Intermediate Blocking, and Cake Filtration models. Data is the average of two runs with error bars of standard error.

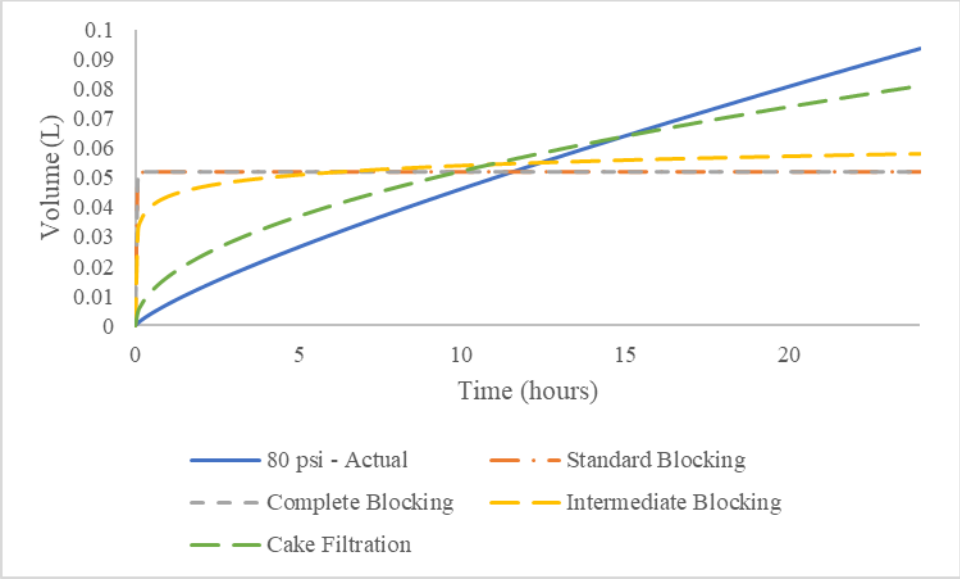

Figure 20 Volume versus time of NF270 membrane fouled for 24-hours with 500 mg/L of sodium alginate at a constant pressure of 80 psi compared to Standard Blocking, Complete Blocking, Intermediate Blocking, and Cake Filtration models.

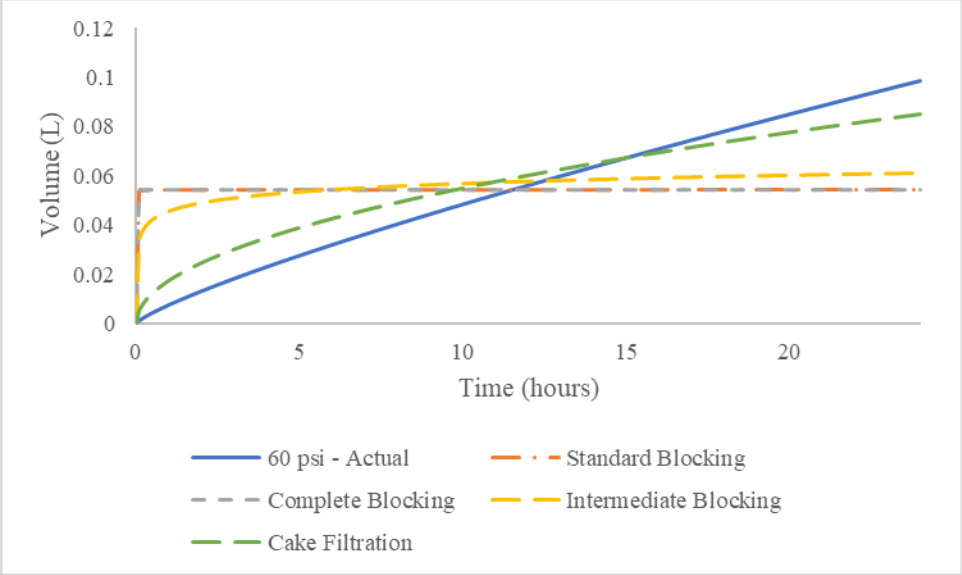

Figure 21 Volume versus time of NF270 membrane fouled for 24-hours with 500 mg/L of sodium alginate at a constant pressure of 60 psi compared to Standard Blocking, Complete Blocking, Intermediate Blocking, and Cake Filtration models.

Table 3 Error of fit and model parameters for the single fouling models: Standard blocking, Complete blocking, Intermediate blocking, and Cake filtration.

Model	Membrane	Pressure (psi)	Model Fit Error, SSR	Model Fit Variance, R^2	Fit Parameter Values
Standard blocking	COF	80	2.425×10^{-1}	0.0142	$K_s = 3.509 \times 10^{1}$ m^{-1}
		60	1.475×10^{-1}	0.0149	$K_s = 4.390 \times 10^{1}$ m^{-1}
	NF270	80	1.914×10^{-1}	0.0149	$K_s = 3.838 \times 10^{1}$ m^{-1}
		60	2.137×10^{-1}	0.0149	$K_s = 3.669 \times 10^{1}$ m^{-1}
Complete blocking	COF	80	2.427×10^{-1}	0.0131	$K_b = 1.195 \times 10^{3}$ hr^{-1}
		60	1.477×10^{-1}	0.0138	$K_b = 1.253 \times 10^{3}$ hr^{-1}
	NF270	80	1.916×10^{-1}	0.0139	$K_b = 1.307 \times 10^{3}$ hr^{-1}
		60	2.139×10^{-1}	0.0136	$K_b = 1.047 \times 10^{3}$ hr^{-1}
Intermediate blocking	COF	80	1.772×10^{-1}	0.2796	$K_i = 1.987 \times 10^{2}$ m^{-1}
		60	1.069×10^{-1}	0.2862	$K_i = 1.987 \times 10^{2}$ m^{-1}
	NF270	80	1.386×10^{-1}	0.2865	$K_i = 2.194 \times 10^{2}$ m^{-1}
		60	1.543×10^{-1}	0.2884	$K_i = 2.053 \times 10^{2}$ m^{-1}
Cake Filtration	COF	80	2.422×10^{-2}	0.9016	$K_c = 6.030 \times 10^{3}$ hr/m^2
		60	1.312×10^{-2}	0.9124	$K_c = 9.499 \times 10^{3}$ hr/m^2
	NF270	80	1.667×10^{-2}	0.9142	$K_c = 7.268 \times 10^{3}$ hr/m^2
		60	1.957×10^{-2}	0.9098	$K_c = 6.626 \times 10^{3}$ hr/m^2

3.4.3 Combine Mechanism Models

$$V = \frac{1}{K_i} ln(1 + \frac{K_i}{K_c J_0}(\sqrt{1 + 2K_c {J_0}^2 t} - 1)) \quad (7)$$

The cake intermediate model (7) combines the cake filtration model and the intermediate blocking model. For the COF membrane experiments at 80 psi and 60 psi, the model fit error was 1.834×10^{-3} and 9.550×10^{-4}, respectively, and the R^2 values were 0.9925 and 0.9936.

For the NF270 membrane experiments at 80 psi and 60 psi, the model fit error was 1.206×10^{-3} and 1.439×10^{-3}, respectively, and the R^2 values were 0.9938 and 0.9934 (Table 4).

$$V = \frac{1}{K_i} ln(1 + \frac{2K_i t}{2 + K_s J_0 t}) \quad (8)$$

The intermediate standard model (8) combines the intermediate blocking model and the standard blocking model. For the COF membrane experiments at 80 psi and 60 psi, the model fit error was 2.402×10^{-1} and 1.462×10^{-1}, respectively, and the R^2 values were 0.0233 and 0.0238. For the NF270 membrane experiments at 80 psi and 60 psi, the model fit error was 1.897×10^{-1} and 2.117×10^{-1}, respectively, and the R^2 values were 0.0239 and 0.0239 (Table 4).

$$V = \frac{J_0}{K_b} (1 - e^{\frac{-K_b}{K_c {J_0}^2} (\sqrt{1 + 2K_c {J_0}^2 t} - 1)}) \quad (9)$$

The cake complete model (9) combines the cake filtration model and the complete blocking model. For the COF membrane experiments at 80 psi and 60 psi, the model fit error was 1.855×10^{-1} and 1.120×10^{-1}, respectively, and the R^2 values were 0.2457 and 0.2520. For the NF270 membrane experiments at 80 psi and 60 psi, the model fit error was 1.451×10^{-1} and 1.626×10^{-1}, respectively, and the R^2 values were 0.2531 and 0.2505 (Table 4).

$$V = \frac{J_0}{K_b} (1 - e^{\frac{-2K_b t}{2 + K_s J_0 t}}) \quad (10)$$

The complete standard model (10) combines the complete blocking model and the standard blocking model. For the COF membrane experiments at 80 psi and 60 psi, the model fit error was 2.402×10^{-1} and 1.462×10^{-1}, respectively, and the R^2 values were 0.0233 and 0.0238. For the NF270 membrane experiments at 80 psi and 60 psi, the model fit error was 1.897×10^{-1} and 2.117×10^{-1}, respectively, and the R^2 values were 0.0238 and 0.0239 (Table 4).

$$V = \frac{2}{K_s} \left(\beta \cos \left(\frac{2\pi}{3} - \frac{1}{3} \cos^{-1}(\alpha) \right) + \frac{1}{3} \right) \quad (11)$$

Wherein,

$$\alpha = \frac{8}{27\beta^3} + \frac{4K_s}{3\beta^3 K_c J_0} - \frac{4{K_s}^2 t}{3\beta^3 K_c}$$

$$\beta = \sqrt{\frac{4}{9} + \frac{4K_s}{3K_c J_0} + \frac{2{K_s}^2 t}{3K_c}}$$

The cake standard model (11) combines the cake filtration model and the standard blocking model. For the COF membrane experiments at 80 psi and 60 psi, the model fit error was 2.422×10^{-2} and 1.312×10^{-2}, respectively, and the R^2 values were 0.9015 and 0.9124. For the NF270 membrane experiments at 80 psi and 60 psi, the model fit error was 2.574×10^{-2} and 1.957×10^{-2}, respectively, and the R^2 values were 0.8676 and 0.9096 (Table 4).

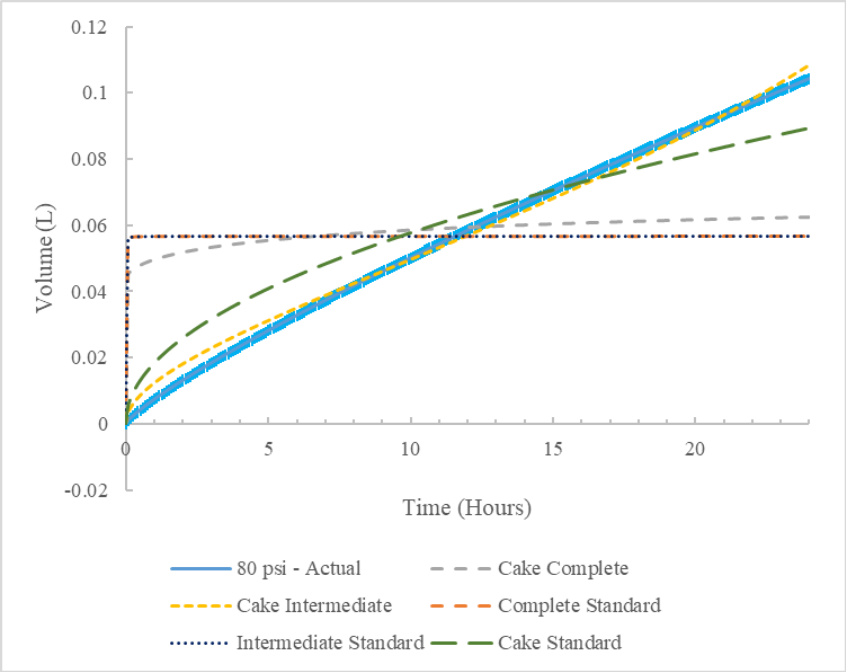

Figure 22 Volume versus time of COF membrane fouled for 24-hours with 500 mg/L of sodium alginate at a constant pressure of 80 psi compared to Cake Intermediate, Intermediate Standard, Cake Complete, Complete Standard, and Cake Standard models. Data is the average of two runs with error bars of standard error.

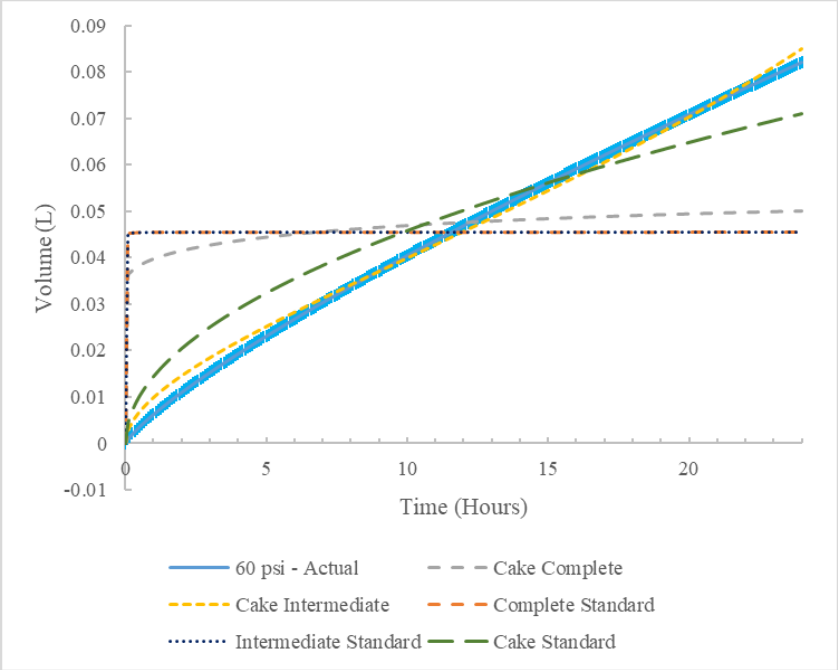

Figure 23 Volume versus time of COF membrane fouled for 24-hours with 500 mg/L of sodium alginate at a constant pressure of 60 psi compared to Cake Intermediate, Intermediate Standard, Cake Complete, Complete Standard, and Cake Standard models. Data is the average of two runs with error bars of standard error.

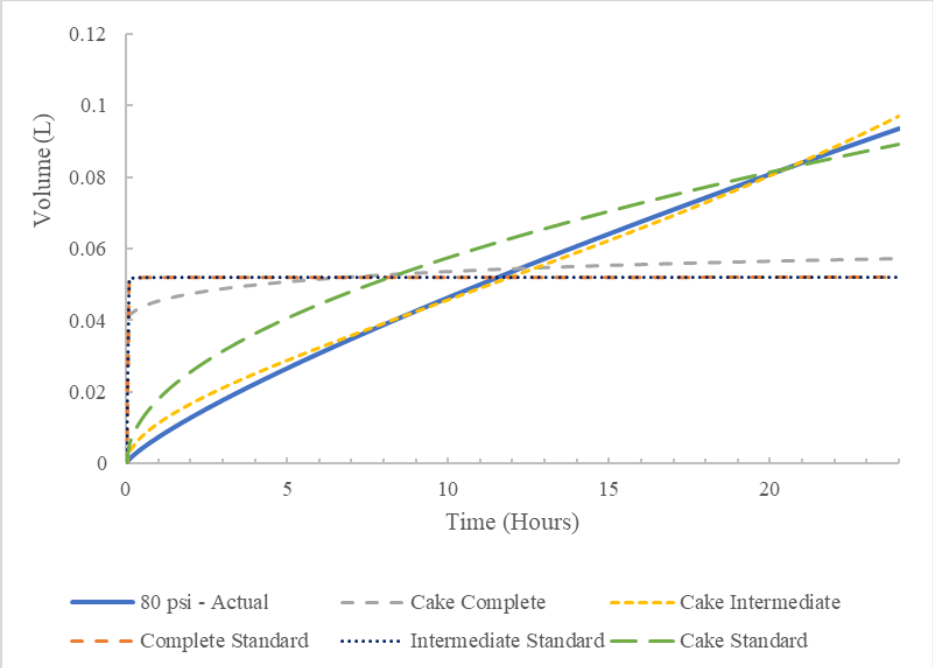

Figure 24 Volume versus time of NF270 membrane fouled for 24-hours with 500 mg/L of sodium alginate at a constant pressure of 80 psi compared to Cake Intermediate, Intermediate Standard, Cake Complete, Complete Standard, and Cake Standard models.

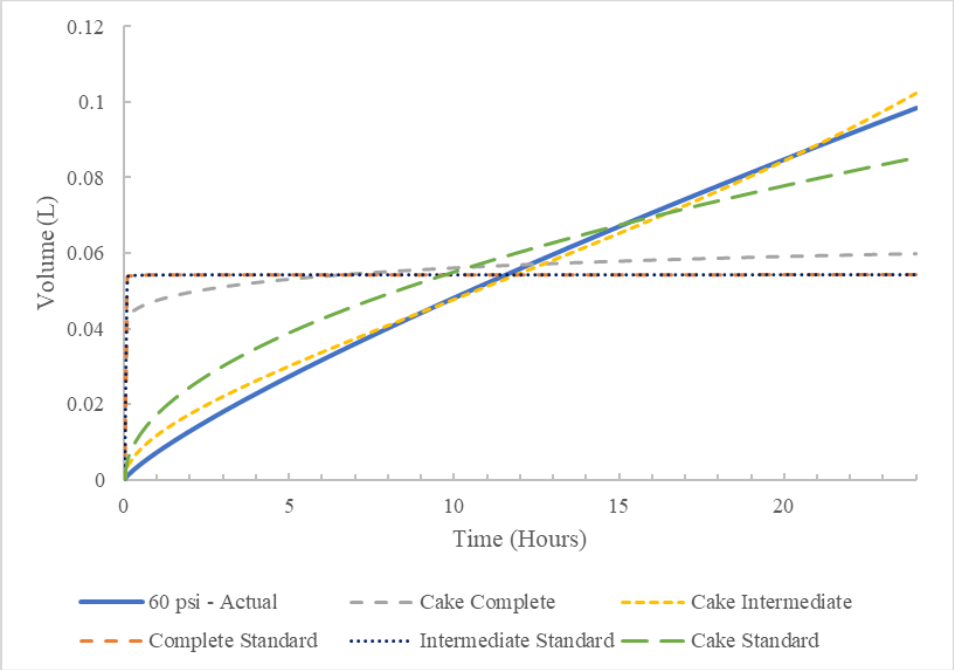

Figure 25 Volume versus time of NF270 membrane fouled for 24-hours with 500 mg/L of sodium alginate at a constant pressure of 60 psi compared to Cake Intermediate, Intermediate Standard, Cake Complete, Complete Standard, and Cake Standard models.

For each experimental dataset, the cake intermediate model was closest to the actual observed data with R^2 values between 0.9925 and 0.9938. Interestingly, the cake standard model and cake filtration models display very similar fits, nearly identical in most cases. This is likely due to a very small K_s values in all cases, indicating and insignificant contribution to the fouling behavior from standard blocking. After cake intermediate, cake filtration (and cake standard by extension) is the next closest fit. These results indicate fouling behavior that is primarily driven by cake filtration, but with some significant contributions from intermediate blocking. Likely, these results indicate that a cake layer formed either simultaneously to, or after an initial stage of, intermediate blocking with pore sealing. This is because intermediate blocking necessarily occurs on the membrane surface, and after a cake layer has formed, new foulant deposits will interact with the surface of the cake layer rather than the surface of the membrane. It is interesting to note

that the modelling results for all experiments were very similar, with no significant differences due to pressure, nor between the types of membranes.

Table 4 Error of fit and model parameters for the combined mechanism models: Cake Intermediate, Intermediate Standard, Cake Complete, Complete Standard, and Cake Standard.

Model	Membrane	Pressure (psi)	Model Fit Error, SSR	Model Fit Variance, R^2	Fit Parameter Values
Cake complete	COF	80	1.855×10^{-1}	0.2457	$K_c = 2.135 \times 10^3$ hr/m^2 $K_b = 9.991 \times 10^2$ hr^{-1}
		60	1.120×10^{-1}	0.2520	$K_c = 7.108 \times 10^3$ hr/m^2 $K_b = 1.049 \times 10^3$ hr^{-1}
	NF270	80	1.451×10^{-1}	0.2531	$K_c = 2.437 \times 10^3$ hr/m^2 $K_b = 1.094 \times 10^3$ hr^{-1}
		60	1.626×10^{-1}	0.2505	$K_c = 4.971 \times 10^3$ hr/m^2 $K_b = 8.762 \times 10^2$ hr^{-1}
Cake intermediate	COF	80	1.834×10^{-3}	0.9925	$K_c = 1.588 \times 10^4$ hr/m^2 $K_i = 1.436 \times 10^1$m^{-1}
		60	9.550×10^{-4}	0.9936	$K_c = 2.379 \times 10^4$ hr/m^2 $K_i = 1.703 \times 10^1$ m^{-1}
	NF270	80	1.206×10^{-3}	0.9938	$K_c = 1.804\times 10^4$ hr/m^2 $K_i = 1.475 \times 10^1$ m^{-1}
		60	1.439×10^{-3}	0.9934	$K_c = 1.680 \times 10^4$ hr/m^2 $K_i = 1.443 \times 10^1$ m^{-1}
Complete standard	COF	80	2.402×10^{-1}	0.0233	$K_b = 2.227 \times 10^0$ hr^{-1} $K_s = 3.516 \times 10^1$ m^{-1}
		60	1.462×10^{-1}	0.0238	$K_b = 3.377 \times 10^0$ hr^{-1} $K_s = 4.392 \times 10^1$ m^{-1}
	NF270	80	1.897×10^{-1}	0.0238	$K_b = 2.227 \times 10^0$ hr^{-1} $K_s = 3.845 \times 10^1$ m^{-1}
		60	2.117×10^{-1}	0.0239	$K_b = 3.377 \times 10^0$ hr^{-1} $K_s = 3.673 \times 10^1$ m^{-1}

Intermediate standard	COF	80	2.402×10^{-1}	0.0233	$K_i = 1.006 \times 10^{-1}$ m^{-1} $K_s = 3.509 \times 10^{1}$ m^{-1}
		60	1.462×10^{-1}	0.0238	$K_i = 1.006 \times 10^{-1}$ m^{-1} $K_s = 4.392 \times 10^{1}$ m^{-1}
	NF270	80	1.897×10^{-1}	0.0239	$K_i = 1.006 \times 10^{-1}$ m^{-1} $K_s = 3.838 \times 10^{1}$ m^{-1}
		60	2.117×10^{-1}	0.0239	$K_i = 1.006 \times 10^{-1}$ m^{-1} $K_s = 3.669 \times 10^{1}$ m^{-1}
Cake standard	COF	80	2.422×10^{-2}	0.9015	$K_c = 3.796 \times 10^{3}$ hr/m^2 $K_s = 9.920 \times 10^{-5}$ m^{-1}
		60	1.312×10^{-2}	0.9124	$K_c = 5.980 \times 10^{3}$ hr/m^2 $K_s = 8.920 \times 10^{-3}$ m^{-1}
	NF270	80	2.574×10^{-2}	0.8676	$K_c = 3.796 \times 10^{3}$ hr/m^2 $K_s = 9.920 \times 10^{-5}$ m^{-1}
		60	1.957×10^{-2}	0.9096	$K_c = 4.170 \times 10^{3}$ hr/m^2 $K_s = 8.920 \times 10^{-3}$ m^{-1}

3.5 Limiting Flux

Critical flux is a theoretical concept in which there is some flux in a membrane system, independent of the initial flux, below which fouling, and flux decline become insignificant [27]. The limiting flux is the pseudo-steady flux which is reached in a real-world membrane system with which fouling, and flux decline nearly ceases. As shown in sec. 3.3, the vast majority of flux decline in all observed cases occurred in the initial 15-minutes, after which the flux decline had significantly slowed. In this case, the limiting flux will be referring to the final flux after the full

24-hour fouling period. Comparing these final "limiting" flux values is valuable to see what factors may affect the limiting flux in a high-concentration organic fouling situation.

In NF270 experiments using constant pressures of 40 psi, 60 psi, and 80 psi, the average final flux after 24-hours of fouling with 500 milligrams per liter sodium alginate was 1.42×10^1 LMH with no relationship found between pressure and final flux. In COF experiments using constant pressures of 60 and 80 psi, the average final flux in the same fouling scenario was 1.42×10^1 LMH. More data is needed to determine if a relationship exists in this case between pressure and final flux. Figure 26 shows a summary of all final flux values.

These results indicate that the foulant-foulant interaction forces may play a bigger role in determining the limiting flux in this scenario than the membrane-foulant interaction forces because there is no significant difference seen between the two types of membranes. As discussed in section 3.4 Fouling Mechanism Modelling, cake filtration was a primary fouling mechanism at play. Given this context, the cake layer's interaction with the depositing foulant likely played a large role in determining the limiting flux.

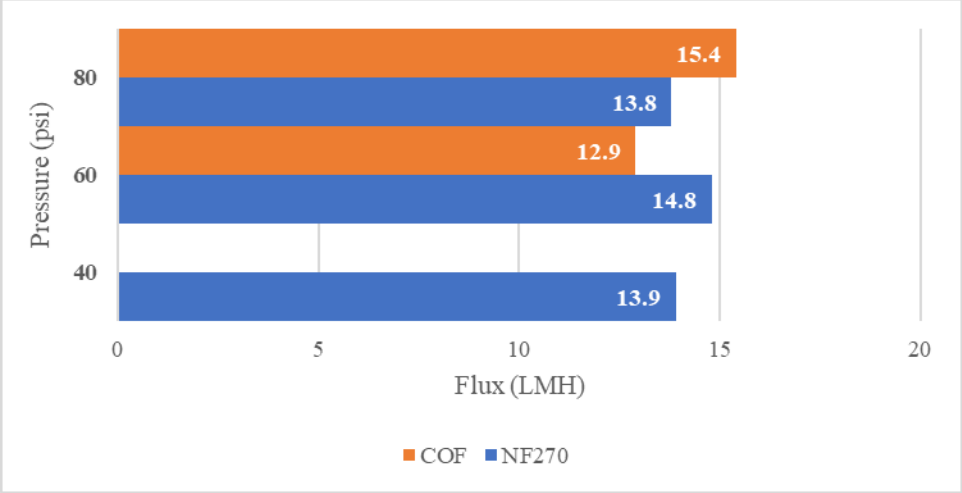

Figure 26 Summary of Final Flux ("limiting flux") values at various constant pressures after 24-hours of organic fouling by 500 mg/L sodium alginate in NF270 and COF membranes. COF membrane datapoints are the average of two datasets with

Chapter 4: Conclusions and Recommendations

4.1 Conclusions

Very little variation was found in the several analyses conducted based on the type of membrane assessed or the pressure used. During fouling with a high-concentration of organic foulant solution – 500 milligrams per liter of sodium alginate in this case – much of the fouling behavior presented independent of these changing variables. The fouling mechanism models for all tested membranes at all tested pressures yielded similar results. In all cases, while cake filtration was found to be the primary fouling mechanism, intermediate pore blocking appeared to also play a role. Ultimately, the combined cake-intermediate model (combining the models for cake filtration and intermediate blocking) produced results most consistent with the experimental data in all cases.

During each experiment, the vast majority of the flux decline (fouling rate) was observed during the initial several minutes of the organic fouling period. This initial period – stage 1 – was taken as the first fifteen minutes of each fouling period to compare each experiment. The flux decline during stage 1 was greater in the NF270 membranes than the COF membranes, but no significant difference was seen between the two membranes during stage 2 (the final 23.75 hours of the fouling period). Additionally, while the fouling rate increased with increasing pressure in both tested membranes during stage 1, no significant relationship was observed between fouling rate and pressure during stage 2.

Finally, there was no relationship observed between the final flux after the 24-hour fouling period and type of membrane, nor pressure. Likely, the limiting flux in these cases in determined primarily by the foulant-foulant interaction forces at play. Due to the results of the mechanism modelling completed for these experiments, cake filtration was shown to be a primary mechanism

for the fouling observed. After the cake layer was formed, any additional foulant deposits would interact almost solely with the cake layer, as opposed to with the membrane surface. Thus, any additional flux decline after the formation of the cake layer would be determined by the foulant-foulant forces (the interaction with the cake layer and the foulant), which explains why there is little difference in the final flux values seen between the two types of membranes tested.

Overall, the lab synthesized TpHz membranes performed very similarly to the DuPont NF270 membranes with little variation. The most prominent difference between the two was the initial flux (COF having higher initial fluxes on average), but after compaction, the flux had leveled to values comparable to the NF270, and thus was not a defining characteristic by the time the foulant was added. Further studies may reveal more similarities or differences between the two membranes. Additional foulants should be tested in each membrane to compare behavior. The current capability of the experimental setup limits the range of pressures that can be tested, but with the additional of additional pumps, perhaps future studies can capture fouling behavior at higher pressures as well.

4.2 Recommendations and Future Work

Several steps can be taken to progress this research further. Firstly, these experiments can be repeated with additional foulants. As discussed in chapter 1, there are several different categories of foulants. This study focused on sodium alginate, which is a brown algae-based polysaccharide that acts as an organic foulant. Because the COF membrane tested is a novel technology, it will also be important to see its behavior with the addition of other foulants, like an inorganic foulant.

It would also be advantageous to explore higher-pressure scenarios. The highest pressure tested was 80 psi due to limitations of the lab setup, but with additional pumps or a higher-powered

pump, higher stable pressures could be reached. Lower pressure scenarios may be tested as well but may not provide as valuable data if much lower than pressures seen in real-world scenarios. The actual pressures used in real-world membrane systems should be considered when determining experimental pressures. Additionally, all experiments in this study were conducted at constant pressure, variable flux scenarios. Future experiments could explore constant flux, variable pressure scenarios.

Finally, limiting flux and critical flux should be further explored. Given that a quasi-steady state was reached during all fouling experiments in this study, additional experiments could be conducted using the same foulant concentration, feedwater chemistry, and membranes, but with a controlled initial flux below the experimentally determined "limiting flux." It was hypothesized that if the initial flux was below the limiting flux, flux decline in the system would remain insignificant. This hypothesis could be the basis for a new study using the same materials and experimental setup.

References

[1] L. K. Wang, P. Jiaping, Y.-T. Hung and N. K. Shammas, Membrane and Desalination Technologies, vol. 13, Totowa, NJ: Humana Press, 2010, pp. 1-20.

[2] C2ES, "Drought and Climate Change," Center for Climate and Energy Solutions, 18 April 2023. [Online]. Available: https://www.c2es.org/content/drought-and-climate-change/. [Accessed 20 April 2023].

[3] Y. Zhou and R. S. Tol, "Evaluating the costs of desalination and water transport," *Water Resources Research,* vol. 41, no. 3, 2005.

[4] J. R. Ziolkowska and R. Reyes, "Prospects for Desalination in the United States - Experience from California, Florida, and Texas," in *Competition for Water Resources: Experiences and Management Approaches in the US and Europe*, 2017, pp. 298-316.

[5] Water Desalination Act of 1996, *Pub. L. No. 104-298, 110 Stat. 3622,* 1996.

[6] *Infrastructure Investment and Jobs Act of 2021,* 2021.

[7] United States Bureau of Reclamation, "About DWPR," 2022. [Online]. Available: https://www.usbr.gov/research/dwpr/about.html.

[8] NIDIS, "California," National Integrated Drought Information System, 20 April 2023. [Online]. Available: https://www.drought.gov/states/california. [Accessed 20 April 2023].

[9] NIDIS, "Florida," National Integrated Drought Information System, 20 April 2023. [Online]. Available: https://www.drought.gov/states/florida. [Accessed 20 April 2023].

[10] J. Donald and S. Grubbs, "Drought in Texas," *Fiscal News,* December 2022.

[11] W. Guo, H. Ngo and J. Li, "A mini-review on membrane fouling," *Bioresource technology,* pp. 27-34, 2012.

[12] A. Hodges, K. Hansen and D. McLeod, "Economics of Bulk Water Transport in Southern California," *Resources,* vol. 3, no. 4, pp. 703-720, 2014.

[13] A. Mohammad, Y. Teow, W. Ang, Y. Chung, D. Oatley-Radcliffe and N. Hilal, "Nanofiltration membranes review: Recent advances and future prospects," *Desalination,* vol. 356, pp. 226-254, 2015.

[14] J. Wang, L. Wang, R. Miao, L. Lv, X. Wang, X. Meng, R. Yang and X. Zhang, "Enhanced gypsum scaling by organic fouling layer on nanofiltration membrane: Characteristics and mechnanisms," *Water Research,* vol. 91, pp. 203-213, 2016.

[15] C. K. Diawara, "Nanofiltration Process Efficiency in Water Desalination," *Separation & Purification Reviews,* pp. 303-325, 2008.

[16] M. K. Wafi, N. Hussain, O. E.-S. Abdalla, M. D. Al-Far, N. A. Al-Hajaj and K. F. Alzonnikah, "Nanofiltration as a cost-saving desalination process," *SN Applied Sciences,* vol. 1, p. 751, 2019.

[17] S.-Y. Ding and W. Wang, "Covalent organic frameworks (COFs): from design to applications," *Chemical Society Reviews,* no. 2, 2013.

[18] S. Yuan, X. Li, J. Zhu, G. Zhang, P. V. Puyvelde and B. Van der Bruggen, "Covalent organic frameworks for membrane separation," *Chemical Society Reviews,* no. 10, 2019.

[19] L.-C. Lin, J. Choi and J. C. Grossman, "Two-dimensional covalent triazine framework as an ultrathin-film nanoporous membrane for desalination," *Chemical Communications,* no. 80, 2015.

[20] K. Zhang, Z. He, K. Gupta and J. Jiang, "Computational design of 2D functional covalent–organic framework membranes for water desalination," *Environmental Science: Water Research & Technology,* no. 4, 2018=7.

[21] L. D. Tijing, Y. C. Woo, J.-S. Choi, S. Lee, S.-H. Kim and H. K. Shon, "Fouling and its control in membrane distillation - A review," *Journal of Membrane Science,* vol. 475, pp. 215-244, 2015.

[22] C. Y. Tang, Q. S. Fu, C. S. Criddle and J. O. Leckie, "Effect of Flux (Transmembrane Pressure) and Membrane Properties on Fouling and Rejection of Reverse Osmosis and Nanofiltration Membranes Treating Perluorooctane Sulfonate Containing Wastewater," *Environmental Science and Technology,* vol. 41, pp. 2008-2014, 2007.

[23] A. Robles, M. V. Ruano, A. Charfi, G. Lesage, M. Heran, H. Jerome, A. Seco, J.-P. Steyer, D. J. Batstone and J. Kim, "A review on anaerobic membrane bioreactors (AnMBRs) focused on modelling and control aspects," *Bioresource Technology,* vol. 270, pp. 612-626, 2018.

[24] G. Bolton, D. LaCasse and R. Kuriyel, "Combined models of membrane fouling: Development and application to microfiltration and ultrafiltration of biological fluids," *Journal of ,* vol. 277, pp. 75-84, 2006.

[25] J. Hermia, "Constant pressure bloking filtration laws - application to power-law non-newtonian fluids," *Institution of Chemical Engineers,* vol. 60, pp. 183-187, 1982.

[26] H. Xu, X. Wang, S. Liang, W. Chunhai, X. Wen and X. Huang, "Outlining the Roles of Membrane-Foulant and Foulant-Foulant Interactions in Organic Fouling During Microfiltration and Ultrafiltration: A Mini-Review," *Frontiers in Chemistry,* vol. 8, p. 417, 2020.

[27] C. Y. Tang and J. O. Leckie, "Membrane Independent Limiting Flux for RO and NF Membranes Fouled by Humic Acid," *Environmental Science and Technology,* vol. 41, pp. 4767-4773, 2007.

[28] P. Bacchin, P. Aimar and R.W. Field, "Critical and sustainable fluxes: Theory, experiments and applications," *Journal of Membrane Science,* vol. 281, pp. 42-69, 2006.

[29] L. Qilin and E. Menachem, "Organic Fouling and Chemical Cleaning of Nanofiltration Membranes: Measurements and Mechanisms," *Environmental Science & Technology,* 2004.

[30] I.-S. Chang, P. Le Clech, B. Jefferson and S. Judd, "Membrane Fouling in Membrane Bioreactors for Wastewater Treatment," *Journal of Environmental Engineering,* vol. 128, no. 11, pp. 1018-1029, 2022.

[31] Y.-N. Wang and C. Y. Tang, "Fouling of Nanofiltration, Reverse Osmosis, and Ultrafiltration Membranes by Protein Mixtures: The Role of Inter-Foulant-Species Interaction," *Environmental Science and Technology,* vol. 45, pp. 6373-6379, 2011.

[32] C. Y. Tang, Y.-N. Kwon and J. O. Leckie, "Fouling of reverse osmosis and nanofiltration membranes by humic acid—Effects of solution composition and hydrodynamic conditions," *Journal of Membrane Science,* vol. 290, pp. 86-94, 2007.

[33] A. A. Mayyahi, "TiO2 Polyamide Thin Film Nanocomposite Reverses Osmosis Membrane for Water Desalination," *Membranes,* vol. 8, no. 3, p. 66, 2018.

[34] M. C. V. Vela, S. A. Blanco, J. L. Garcia and E. B. Rogriguez, "Analysis of membrane pore blocking models applied to the ultrafiltration of PEG," *Seperation and Purification Technology,* vol. 62, pp. 489-498, 2008.

[35] C. Tzotzi, T. Pahiasaki, S. Yiantsios, A. Karabelas and N. Andritsos, "A study of CaCO3 scale formation and inhibition in RO and NF membrane processes," *Journal of Membrane Science,* vol. 296, pp. 171-184, 2007.

Appendix

Model Fit Error, SSE

$$\text{SSE} = \sum_{i=1}^{n} (\widehat{y_i} - y_i)^2$$

Where,

$\widehat{y_i}$ = predicted value;

y_i = experimental value.

Model Fit Variance, R^2

$$R^2 = \frac{\sum_{i=1}^{n} (\widehat{y_i} - \bar{y})^2}{\sum_{i=1}^{n} (y_i - \bar{y})^2}$$

Where,

$\widehat{y_i}$ = predicted value;

y_i = experimental value;

$\bar{y}$ = experimental mean.